creative commons
COMMONS DEED

저작자표시-비영리-변경금지 2.0 대한민국

이용자는 아래의 조건을 따르는 경우에 한하여 자유롭게

- 이 저작물을 복제, 배포, 전송, 전시, 공연 및 방송할 수 있습니다.

다음과 같은 조건을 따라야 합니다:

저작자표시. 귀하는 원저작자를 표시하여야 합니다.

비영리. 귀하는 이 저작물을 영리 목적으로 이용할 수 없습니다.

변경금지. 귀하는 이 저작물을 개작, 변형 또는 가공할 수 없습니다.

- 귀하는, 이 저작물의 재이용이나 배포의 경우, 이 저작물에 적용된 이용허락조건을 명확하게 나타내어야 합니다.
- 저작권자로부터 별도의 허가를 받으면 이러한 조건들은 적용되지 않습니다.

저작권법에 따른 이용자의 권리는 위의 내용에 의하여 영향을 받지 않습니다.

이것은 이용허락규약(Legal Code)을 이해하기 쉽게 요약한 것입니다.

Disclaimer

dCollection

Master's Thesis of Science

Discovery and Characterization of Polymyxin-Resistance Genes PmrE and PmrF from Sediment Microbiome

해양미생물균주에서 추출한 폴리마이신 저항 유전자의 발견과 성질 연구

August 2022

Graduate School of Natural Science
Seoul National University
Chemistry Major

Hwan Jin Joo

Discovery and Characterization of Polymyxin-Resistance Genes PmrE and PmrF from Sediment Microbiome

Woon Ju Song

Submitting a master's thesis of
Science

August 2022

Graduate School of Natural Science
Seoul National University
Chemistry Major

Hwan Jin Joo

Confirming the master's thesis written by
Hwan Jin Joo
August 2022

Chair _____(Seal)
Vice Chair _____(Seal)
Examiner _____(Seal)

Abstract

Polymyxin is a last-line antibiotic used to treat gram-negative pathogens. Thus, the discovery and biochemical characterization of the resistance genes against polymyxin is urgently needed for diagnosis, treatment, and novel antibiotic design. Herein, we report novel polymyxin resistance genes identified from sediment microbiome. Despite their low sequence identity against the known pmrE and pmrF, they show in vitro activities in UDP-glucose oxidation and L-Ara4N transfer to undecaprenyl phosphate, which occur as the part of lipid A modification that leads to polymyxin resistance. The expression of pmrE and pmrF also showed substantially high minimum inhibitory concentrations in the presence of vanadate ions, indicating that they constitute polymyxin resistomes.

Keyword: Polymyxin; antibiotic resistance; metagenome; UDP-glucose dehydrogenase; undecaprenyl-phosphate 4-deoxy-4-formamido-L-arabinose transferase

Student Number: 2019-26052

Table of Contents

Chapter 1. Introduction

1.1. Study Background

Antibiotic resistance poses a global threat to human health. It continuously emerges and rapidly spreads among pathogens, leading to the development of multidrug-resistant bacteria. The acronym "ESKAPE" includes six pathogens that exhibit multidrug resistance and virulence: *Enterococcus faecium, Staphylococcus aureus, Klebsiella pneumoniae, Acinetobacter baumannii, Pseudomonas aeruginosa,* and *Enterobacter spp.* (1, 2). One of the pathogens, *A. baumannii*, had first demonstrated carbapenem resistance in 2000, and was detected nearly everywhere, including the USA, Canada, South America, Europe, Africa, the Middle East, Southeast Asia, and Australia in 2019 (3). As a result, Centers for Disease Control and Prevention reported that more than 2.8 million people were infected by antibiotic-resistant pathogens and 35 thousand people deceased in the USA (4), necessitating the discovery of novel antibiotics to replace pre-existing ones.

However, we have faced the so-called antibiotic resistance paradox (5). If a new antibiotic presented low efficacy, commercial sales would reduce, and with high efficacy, the usage would be restrained to preserve its resistant-free activity. Consequently, the development of novel antibiotics is not profitable for the pharmaceutical industry in both cases, and the number of antibiotics approved by the US Food and Drug Administration has continuously decreased over the past three decades (6).

As an alternative, pre-existing antibiotics with low levels of resistance can be reassessed. Along this line, polymyxins, such as polymyxin B and E (also known as colistin), can be of interest (7-10). They are composed of cyclic and cationic nonribosomal peptides produced by the gram-positive bacterium *Paenibacillus polymyxa* (Figure 1A–B) (11). These secondary metabolites bind to lipopolysaccharide (LPS) on the outer membrane via electrostatic and hydrophobic interactions (12, 13), subsequently disrupting the membranes of gram-negative bacteria (14-16). They were discovered in the 1940s (17), but their use was banned in the 1960s due to nephrotoxicity (18). Thus, the limited usage led polymyxins to be resistance-free antibiotics for 50 years. However, polymyxin-resistant strains were discovered (19-23), indicating that an up-to-date understanding of the antibiotic-resistance genes (24, 25) with polymyxin are required to preserve this last line of antibiotics and effectively

administer them to urgent patients.

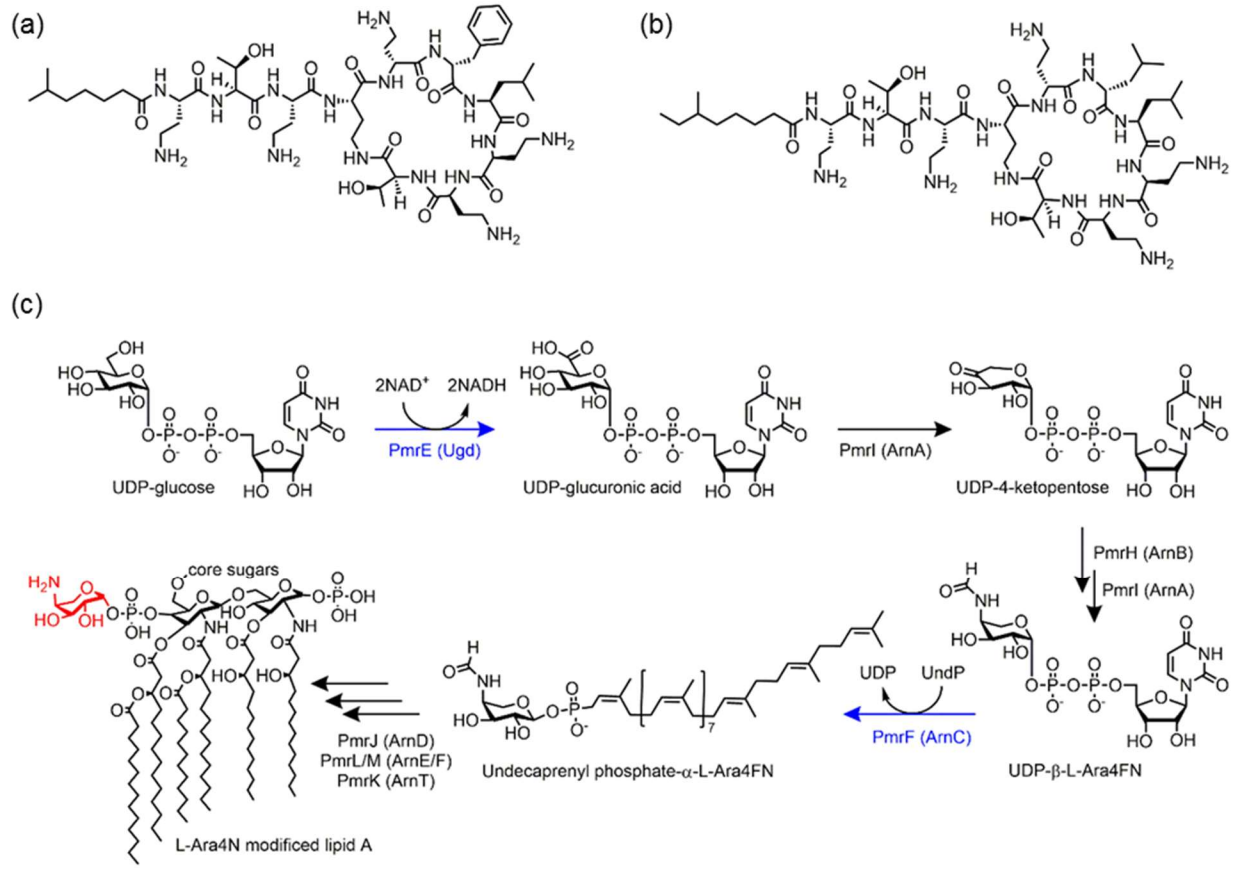

Figure 1. Polymyxin and its antibiotic resistance. The molecular structure of (a) polymyxin B2 and (b) polymyxin E. (c) The modification pathway of Lipid A. L−Ara4N moiety is highlighted in red. The potential reactions that are mediated by the genes of our interest are highlighted in blue.

The proposed molecular mechanism of polymyxin resistance is associated with modifying LPS. Various conditions, such as low pH, low Mg^{2+}, and high Fe^{3+}/Al^{3+}, can function as chemical stimuli (15, 16, 26−28) to two−component systems, PhoP/PhoQ and PmrA/PmrB. Then, they upregulate a series of seven genes in *pmr* operon (*pmrHFIJKLM*) or *arn* operon (*arnBCADTEF*) and *pmrE* (Figure 1C). Then, the gene cluster modifies the phosphate group of lipid A in LPS with a cationic molecule, such as 4−amino−4−deoxy−L−arabinose (L−Ara4N). Consequently, modified lipid A shows substantially weaker interactions with positively charged polymyxins, conferring resistance to polymyxin. Although they are latent under normal cell−growth conditions,

these genes are present in several gram−negative bacteria, suggesting that the activation and emergence of these chemical processes may occur more often and rapidly than expected. Therefore, these genes need to be investigated in advance.

Integrative studies of bioinformatic and biochemical analyses can be a powerful approach to discover and characterize novel genes related to antibiotic resistance (29−31). In particular, the discovery and biochemical validation of articulately sorted genes from metagenomes have allowed us to explore different sequence variations apart from genomes. In addition, biochemical characterization enabled us to validate the chemical activity of novel functional genes.

1.2. Purpose of Research

Herein, we carried out integrated bioinformatics and biochemical analyses of two discrete genes related to polymyxin resistance. We discovered three putative *pmrE* genes and two putative *pmrF* genes from various environmental samples, where both *pmrE* and *pmrF* were involved in modifying LPS, severely weakening the antibiotic action of polymyxins. The resulting *pmrE* was also annotated as uridine-diphosphate glucose dehydrogenase or UDP-glucose 6-dehydrogenase (UGDH) because it catalyzed the sequential oxidation of UDP-glucose into UDP-glucuronic acid (32-36) (Figure 1C). *PmrF* (*arnC* or *yfbF*) was also annotated as undecaprenyl-phosphate 4-deoxy-4-formamido-L-arabinose transferase, which transferred L-Ara4FN group to undecaprenyl phosphate (UndP). We also prepared each gene in *E. coli* (*pmrE1* and *pmrF1*) as a control. The genes were heterologously expressed for biochemical characterization, and their biochemical activities were determined under both *in vitro* and *in vivo* conditions. Our work demonstrated that the discovered genes are chemically competent in modifying lipid A, suggesting potential roles in polymyxin resistance.

Chapter 2. Results and Discussion

2.1. Novel polymyxin resistance genes from sediment microbiome

We collected five putative pmr genes (*pmrE2, pmrE3, pmr4 and pmrF2, pmrF3*) from sediment microbiome samples (Table 1). The *pmrE2, pmrE3, and pmrE4* genes showed 64%, 39%, and 41% sequence identities to *pmrE1*, respectively (Table 2). Sequence network analysis showed that the discovered metagenomic *pmrE* genes were considerably dissimilar from the previously reported UGDHs (Figure 2), suggesting that biochemical studies of these genes may expand the scope of our understanding of UGDH genes. NCBI BLAST sequence analysis indicated that *pmrE2*, *pmrE3*, and *pmrE4* genes are most close to UGDH or nucleotide sugar dehydrogenase from *Celeribacter persicus*, *Candidatus Methanofastidiosum sp.*, and *Pseudoxanthomonas suwonensis*, respectively (78%, 44%, and 45% sequence identity). Notably, the pmrE3 gene is highly similar to the marine metagenome samples collected from the Eastern North American coast to the Eastern Pacific Ocean (93% sequence identity) (37).

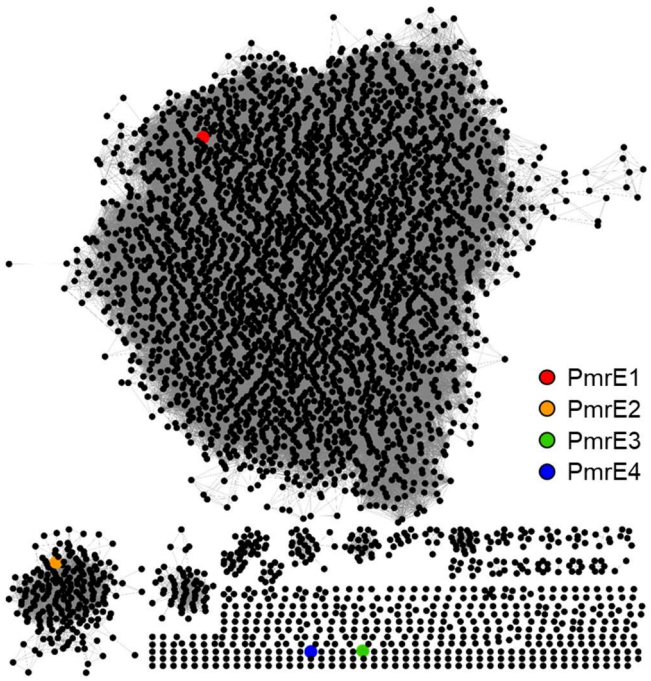

Figure 2. The sequence similarity network analysis of PmrE-like proteins. Each node represents a unique sequence, and each edge represents the pairwise connection between two sequences with sequence identity higher than 80%.

We constructed homology-modeling structures of the putative *pmrE* genes and inspected the sequences and structures of the previously reported UGDHs (Figure 3–4). All the *pmrE1–4* genes showed highly conserved sequence motifs that encoded two active sites to bind substrates, NAD^+ and UDP-glucose. NAD^+-binding site is composed of four sequence motifs: GxGYV, I(A|S)(V|T)(G|P)T(P|D), KST(V|I)P(V|I), and PEFL(R|K|A)EG at the N-terminus (Figure 4B, 4D). The sequence motif for the UDP-glucose-binding site was also preserved in all *pmrE* genes as (Y|F)xx(P|A)(S|G)xG(Y|F)GG at the C-terminus (Figure 4C–D) (34, 35, 38, 39).

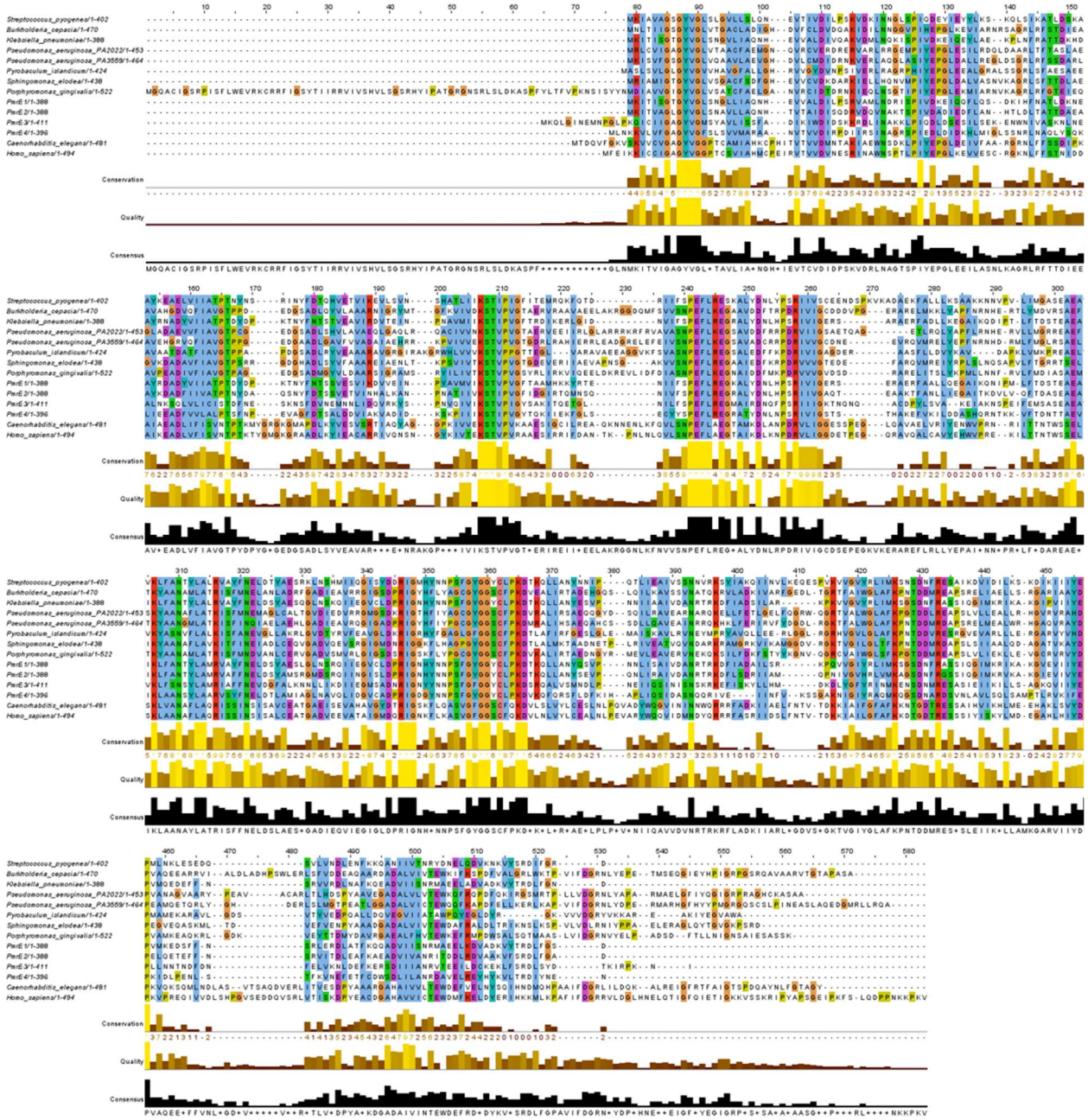

Figure 3. The sequence alignments of PmrE proteins. Previously characterized UGDH proteins were aligned with PmrE1–4 proteins.

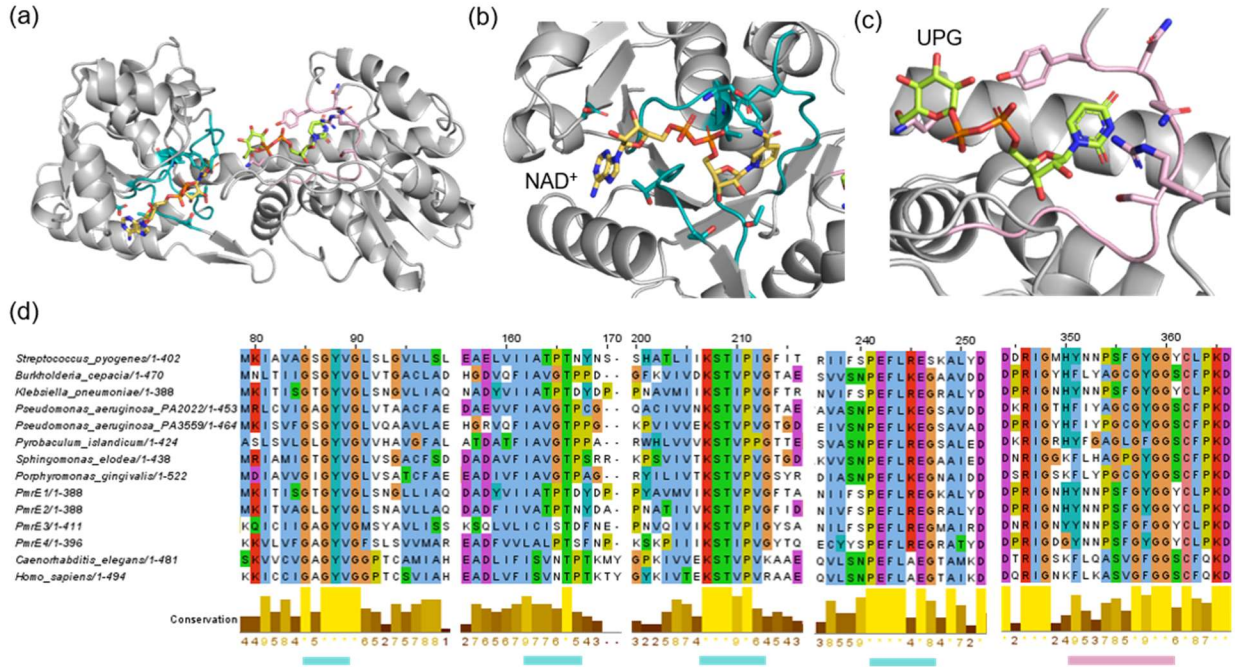

Figure 4. Structure-guided sequence analysis of pmrE1–4 genes. (a) The substrate-binding pocket of PmrE1. The structure was simulated by SWISS-model using the crystal structure of UGDH from Klebsiella pneumoniae (PDB 3PLR) and UDP-glucose from Homo sapiens (PDB 2Q3E). NAD^+ and UDP-glucose-binding domains are colored in cyan and light magenta, respectively. The enlarged region of (b) NAD^+- and (c) UPG-binding domains in (a). (d) Multiple sequence alignment, representing the NAD^+-binding domain (cyan bar) and UDP-glucose-binding domain (light magenta bar).

We also explored the sequences and homology-modeling structures of the putative *pmrF* genes. Few *pmrF*-like genes have been reported to date; only five have been deposited in the UniProtKB sequence database, and they were from *E. coli* or *Yersinia pseudotuberculosis*. In addition, to the best of our knowledge, no biochemical characterization was conducted, not even on the *pmrF* from *E. coli*. In addition, no protein structure of the same EC number as PmrF (EC 2.4.2.53) is available in the RCSB database to date. The *pmrF2* and *pmrF3* genes were similar to glycosyltransferases from *Gammaproteobacteria* and *Chloroflexi* species with a sequence identity of 62% and 72%, respectively. Homology-modeling suggests that PmrF is similar to polyisoprenyl-phosphate glycosyltransferase GtrB from *Synechocystis sp. PCC6803* (PDB 5EKP), which shows 26–32% protein sequence identity to PmrF1–3 (40).

The sequence network analysis was conducted with the homologous *pmrF* and *GtrB*

genes collected from the bacterial genomes and metagenomes. At least four discrete groups of the *pmrF* genes were clustered (Figure 5A). Weblogo analysis of individually clustered genes revealed at least six sequence motifs highly conserved (Figure 5B–C and Figure 6), and they were tentatively assigned as Mg^{2+}−binding site (DxD), UndP−binding site (R122 and R200 in GtrB numbering), and UDP−glucose−binding site (Px(Y|F) and (F|Y)G(Q|K)) (40). Notably, catalytic aspartate, which functions as a Lewis acid in GtrB (D157), was not observed in PmrF1–3, although there was a conserved aspartate at the −4 position (Figure 5C). Alternatively, they might not require such an acidic residue for glycosyltransferase activity, as suggested for the dolichylphosphate mannose synthase from *Pyrococcus furiosus* (*Pf*DPMS) (41); *Pf*DPMS and GtrB showed similar structures and sequence motifs except D157 in GtrB, and *Pf*DPMS has no acidic residue nearby the active site.

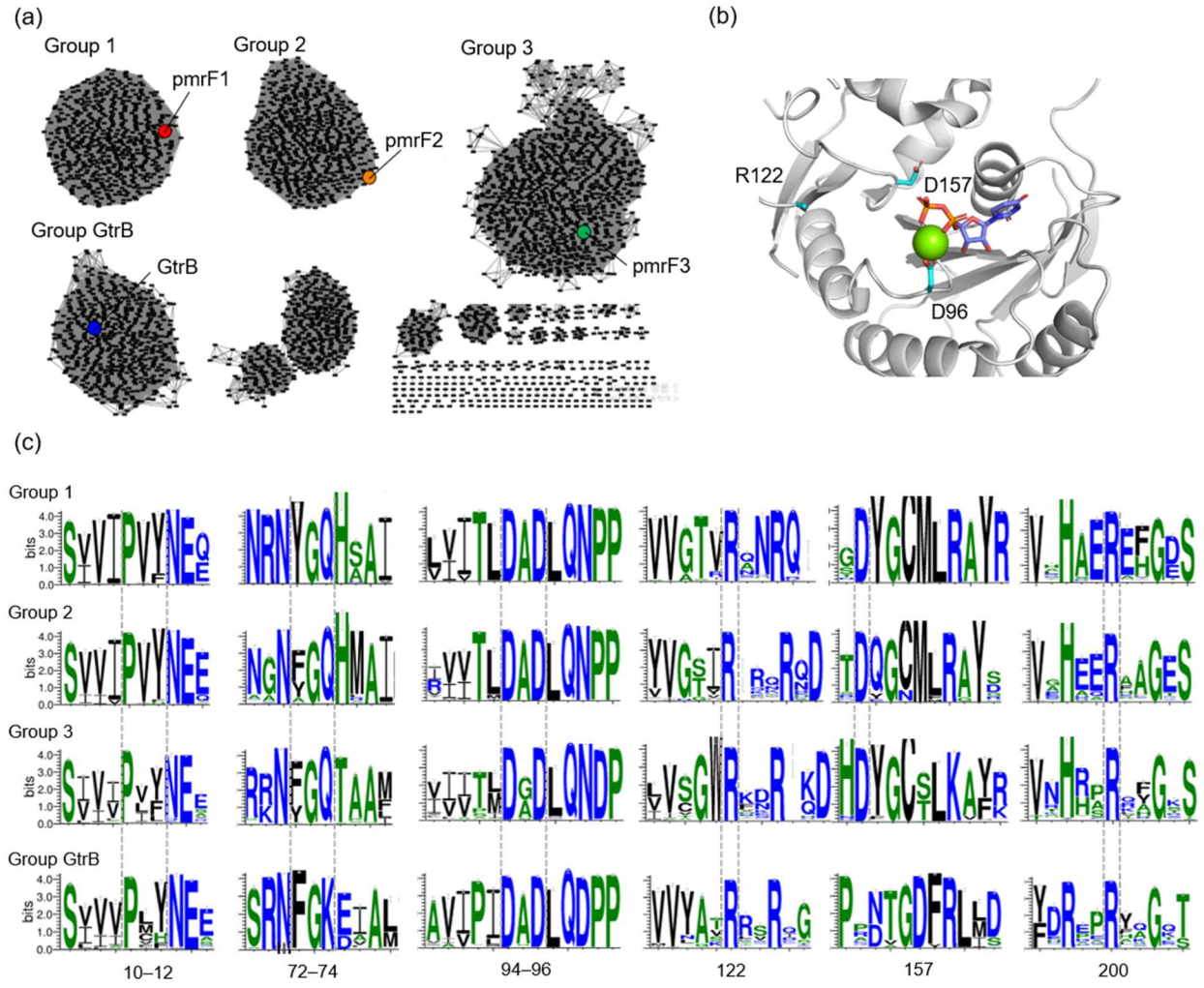

\

Figure 5. Sequence and structure analysis of PmrF-like proteins. (a) Sequence similarity network analysis of PmrF1–3 and GtrB. Each node represents a unique sequence, and each edge represents the pairwise connection between two sequences with an identity higher than 60%. GtrB-like sequences are included for comparison. (b) The active site of GtrB (PDB 5EKE). Catalytically essential residues are represented by cyan sticks. Mg^{2+} cation and UDP molecule are represented with a green sphere and purple sticks, respectively. (c) Weblogo analysis of pmrF-like genes from (a). Conserved essential residues, such as Mg^{2+}-binding site (DxD in residues 94–96 in GtrB numbers), two UndP-binding sites (R122 and R200), catalytic residue (D157), and UPG-binding sites ((Px(Y|F) and (F|Y)G(Q|K) as residues 10–12 and 72–74, respectively) are highlighted with dashed lines.

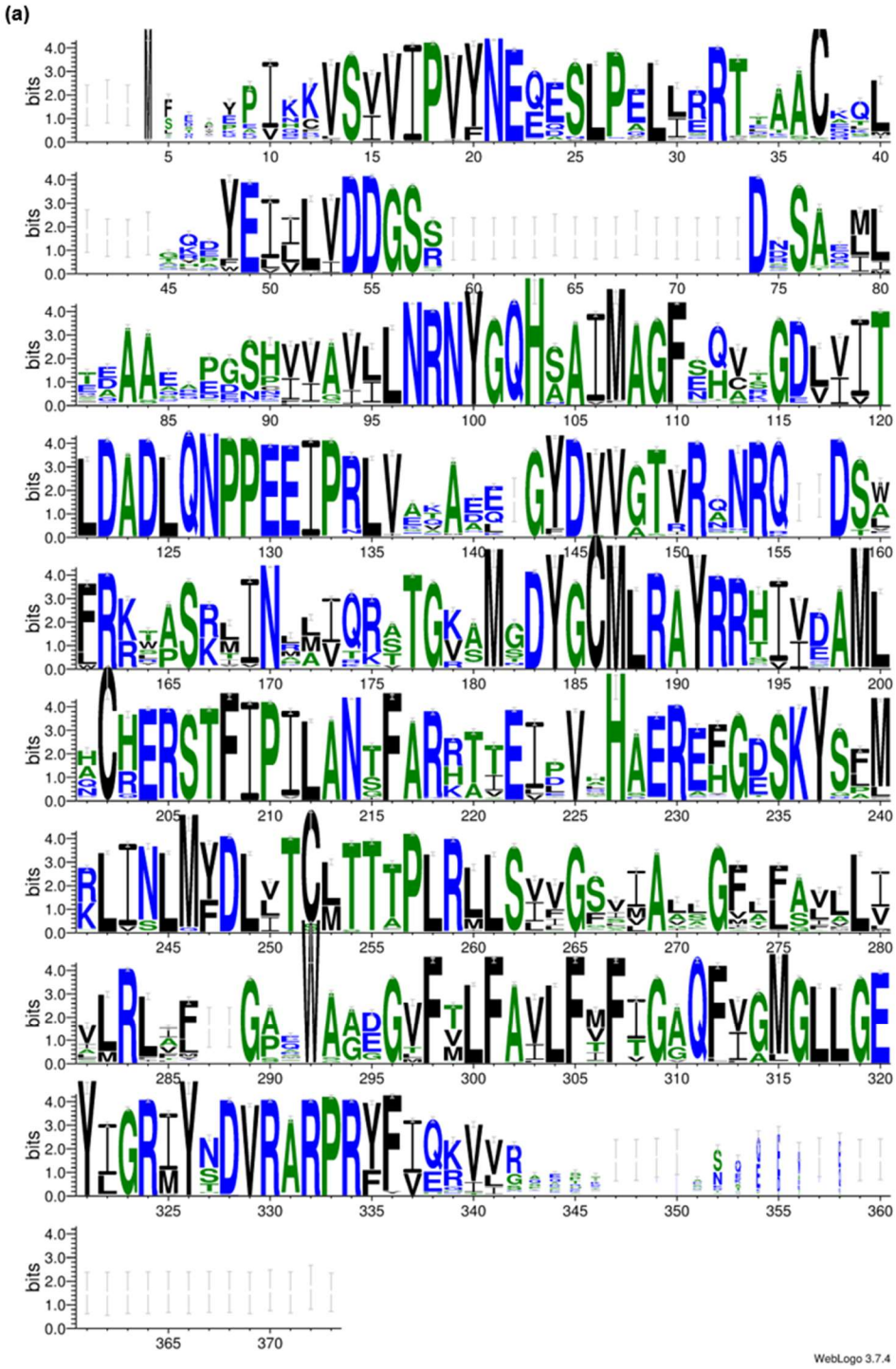
(a)
bits
WebLogo 3.7.4

(b)

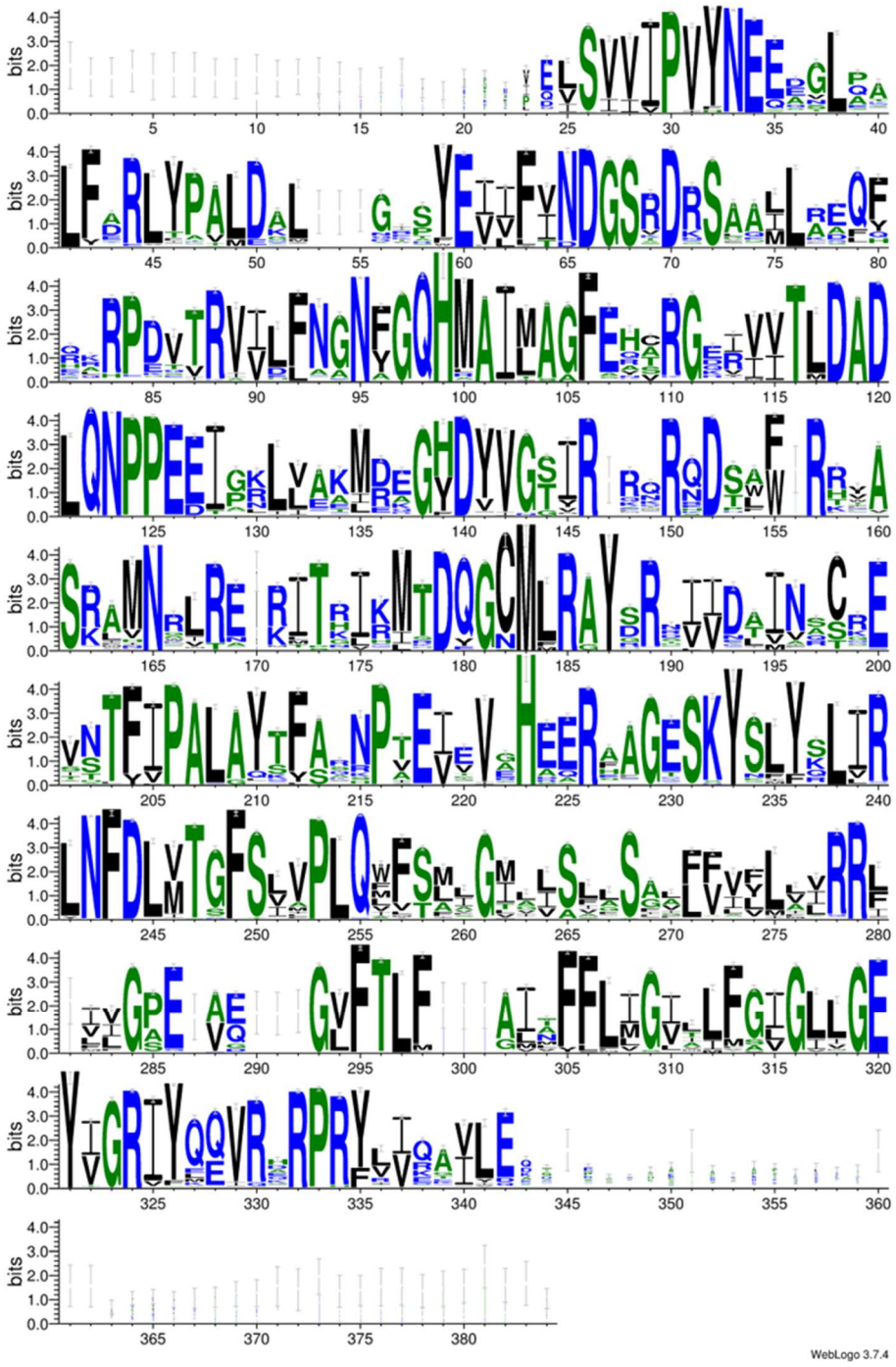
bits
4.0
3.0
2.0
1.0
0.0
5 10 15 20 25 30 35 40
45 50 55 60 65 70 75 80
85 90 95 100 105 110 115 120
125 130 135 140 145 150 155 160
165 170 175 180 185 190 195 200
205 210 215 220 225 230 235 240
245 250 255 260 265 270 275 280
285 290 295 300 305 310 315 320
325 330 335 340 345 350 355 360
365 370 375 380
WebLogo 3.7.4

(c)

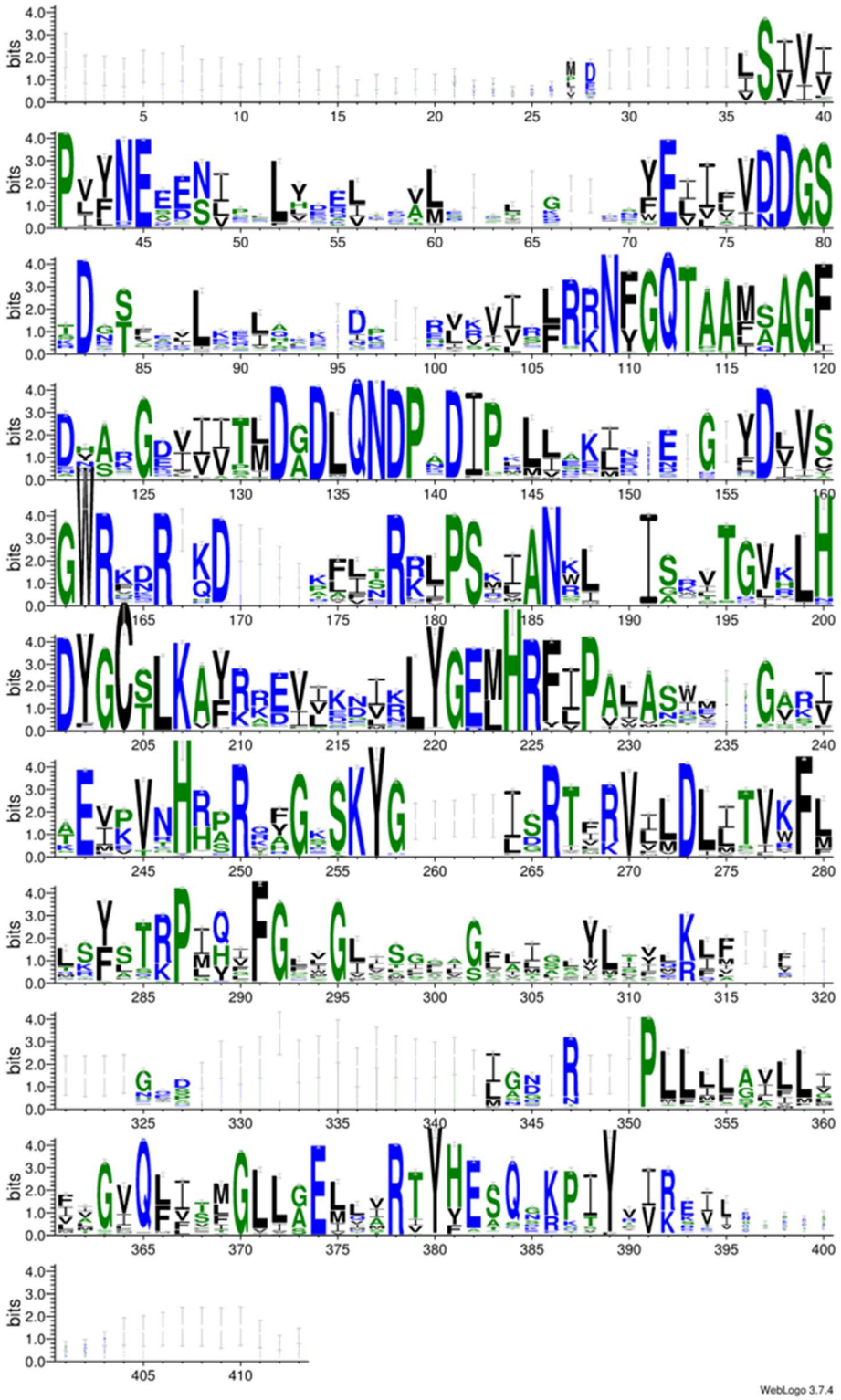

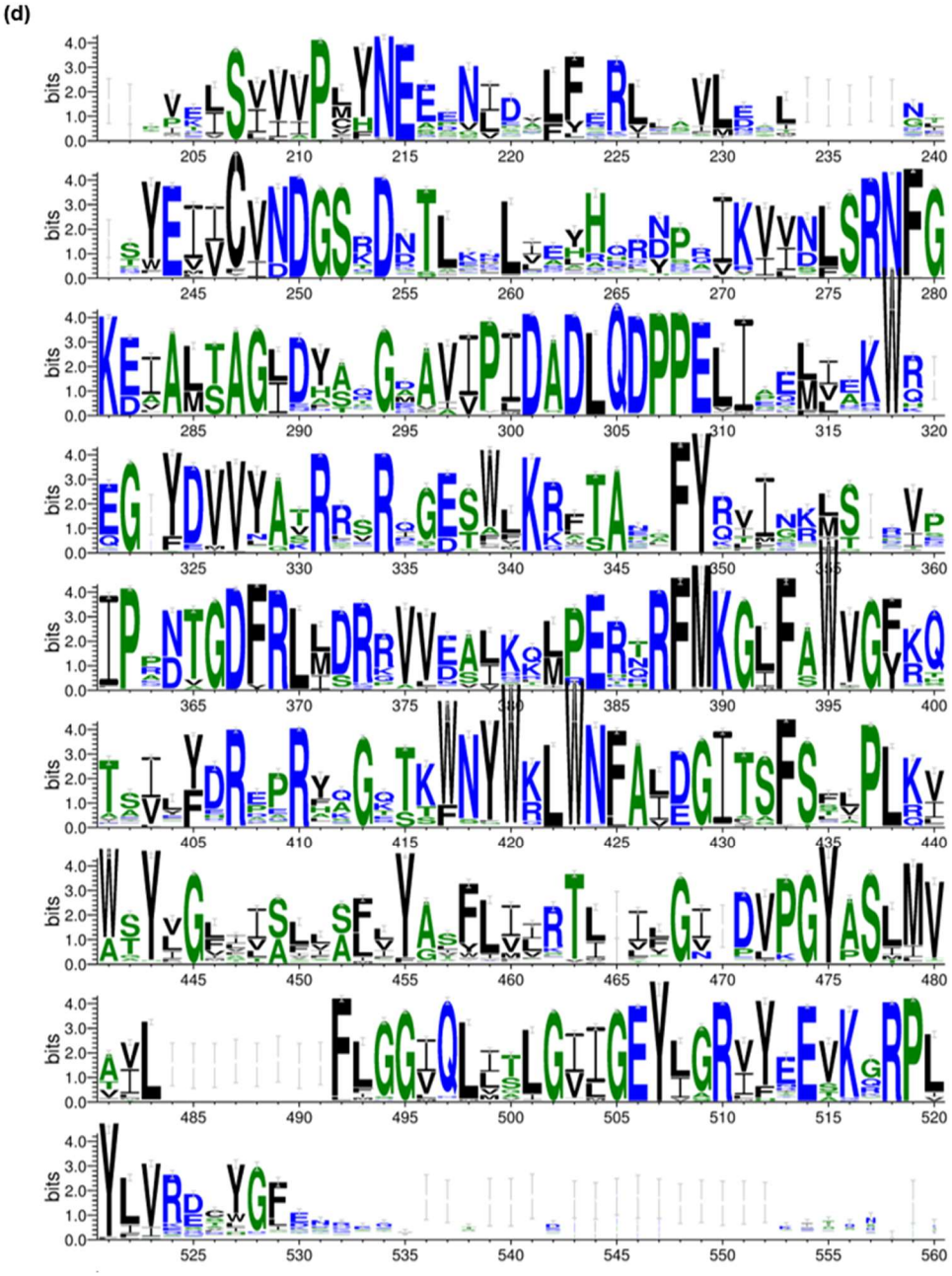

Figure 6. WebLogo frequency plot of amino acids at PmrF-like proteins. A group including (a) PmrF1 (b) PmrF2, (c) PmrF3, and (d) GtrB.

2.2. Expression, isolation, and structural analysis of the pmrE and pmrF genes

Putative PmrE and PmrF proteins were prepared using heterologous expression in *E. coli* (Figure 7–10). After purification, we validated the oligomeric states of PmrE1–4 and PmrF1–3 by size–exclusion chromatography with calibration curve of known protein (Figure 11). It has been reported that substrate/product–binding or mutations of UGDHs (34, 42) may alter oligomeric states and induce substantial conformational changes, suggesting that structural features of PmrE proteins might govern their biochemical functions.

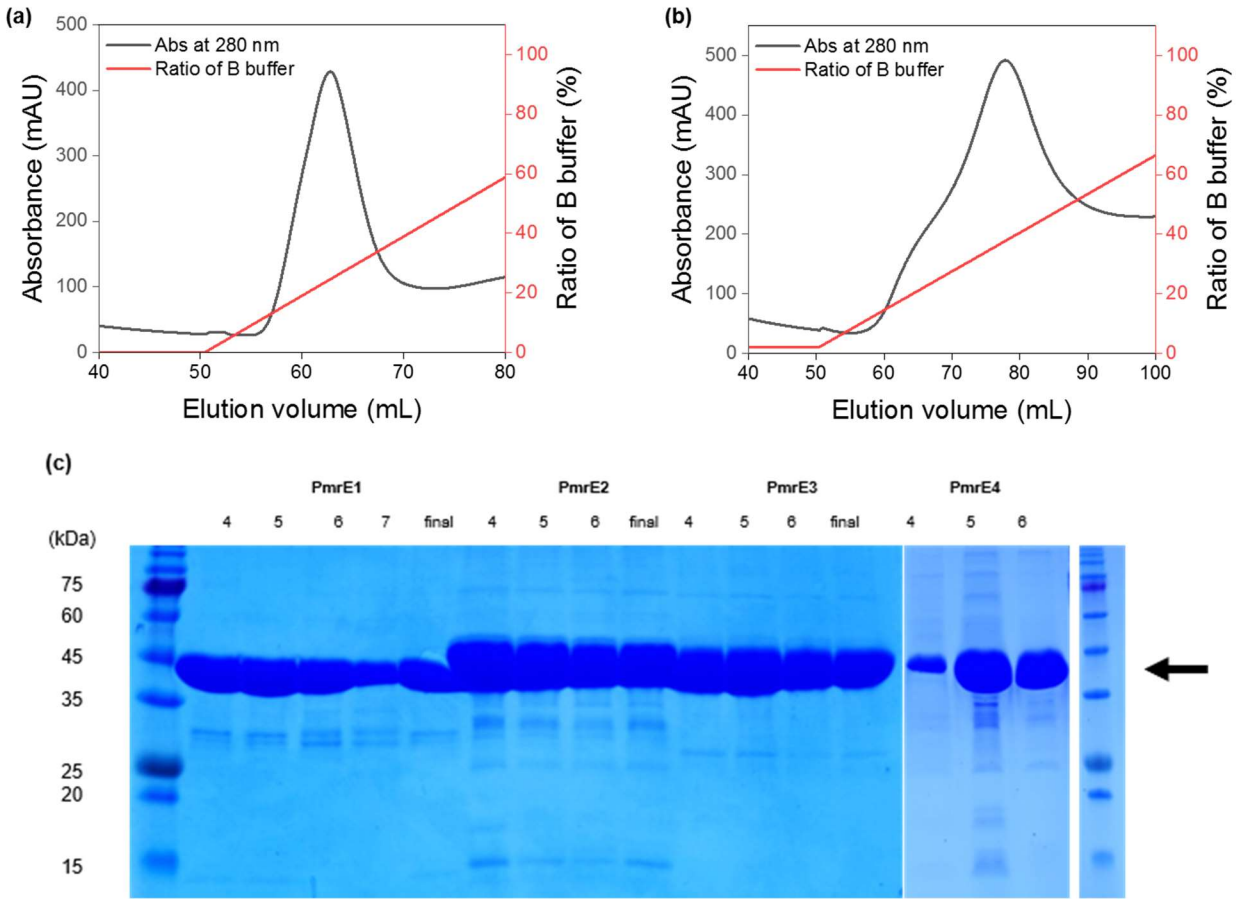

Figure 7. The purification of PmrE proteins. The representative FPLC traces of (a) PmrE1 and (b) PmrE2 in Ni–affinity chromatography and (c) SDS–PAGE analysis of the purified PmrE1–4 proteins. The arrow indicates the size of the desired proteins.

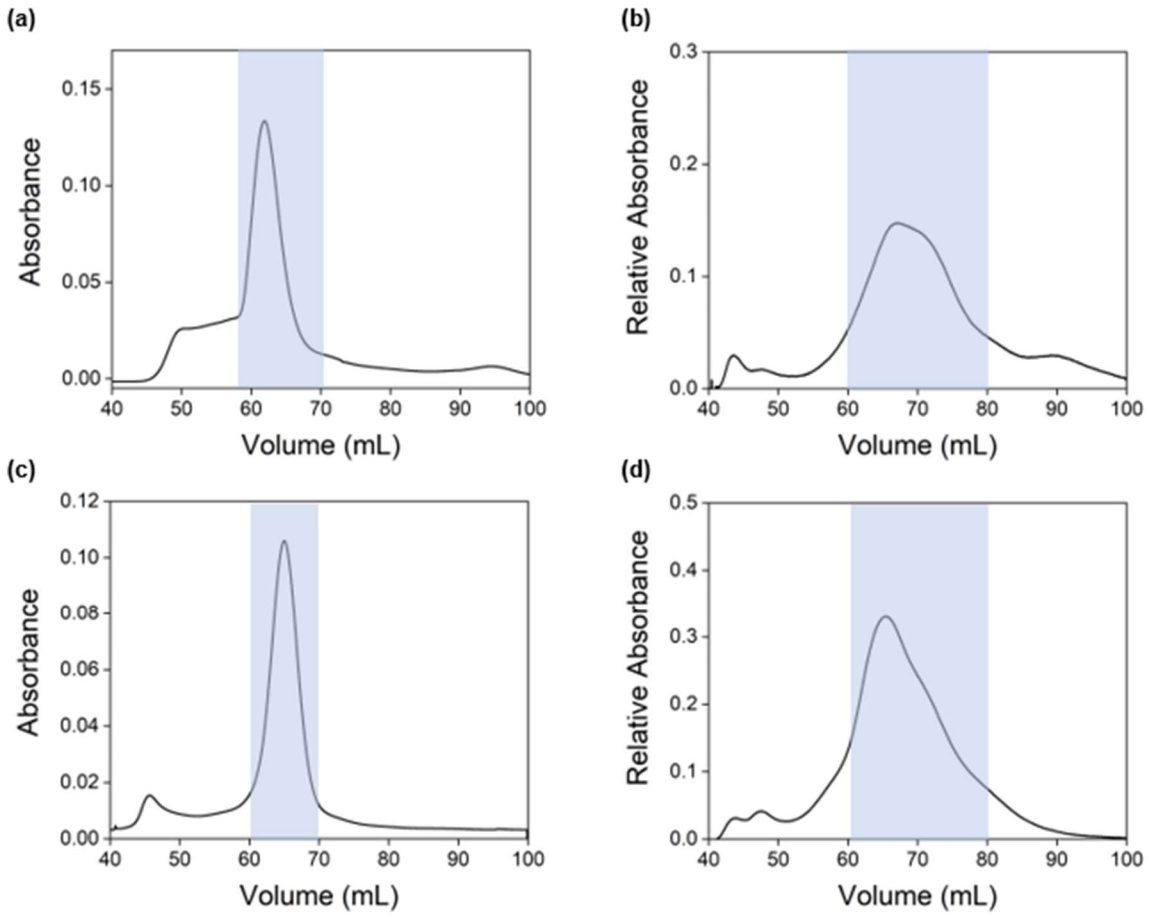

Figure 8. The size-exclusion chromatography of PmrE proteins. (a) PmrE1 (b) PmrE2 (c) PmrE3 (d) PmrE4. The highlighted fractions were used for the activity assays.

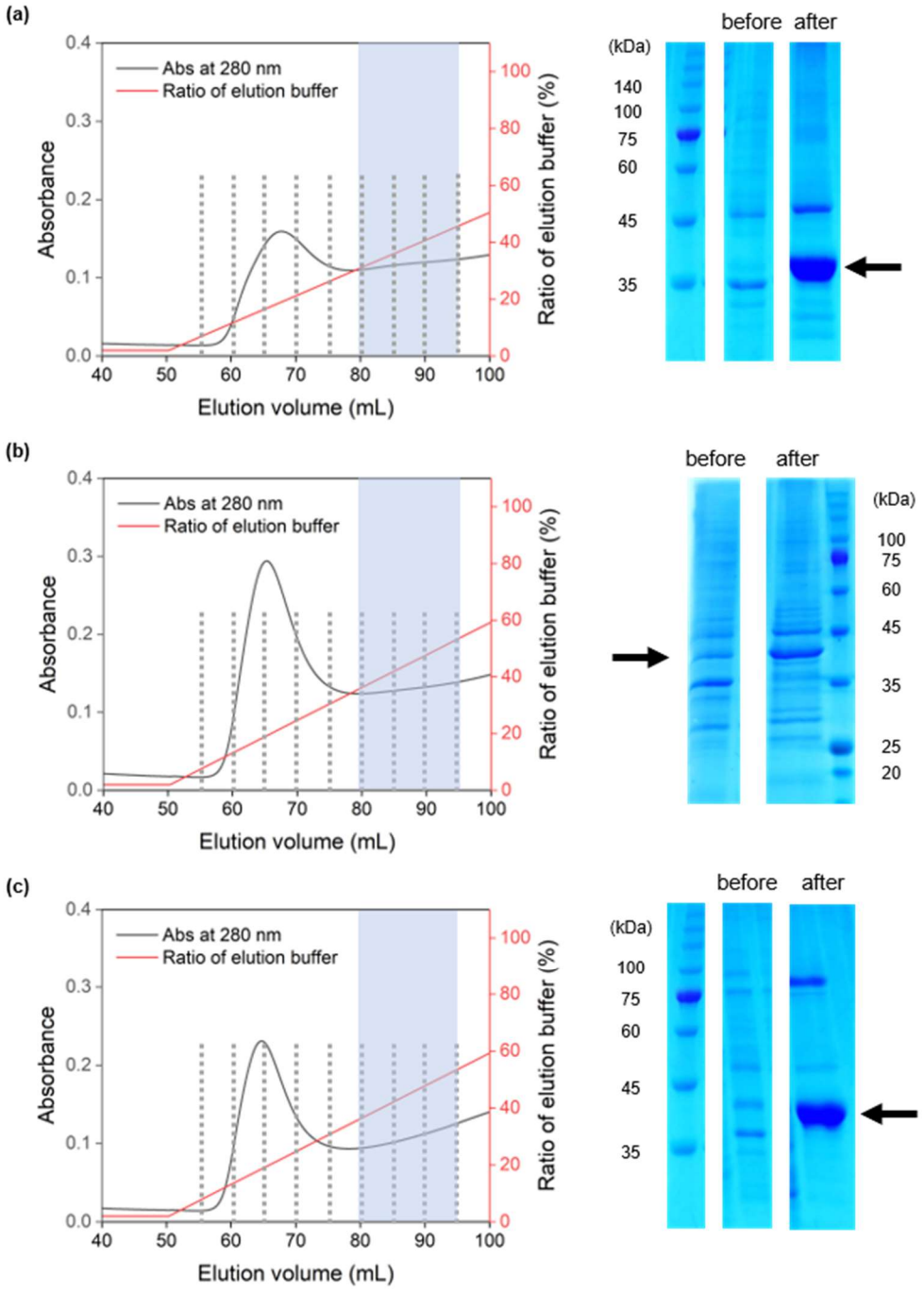

Figure 9. Purification of PmrF1–3 proteins. (a) PmrF1 (b) PmrF2 (c) PmrF3. (left) Representative FPLC traces in His-tag affinity chromatography (right) SDS-PAGE analysis before and after purification shown in (a). The arrows indicate the size of the desired proteins.

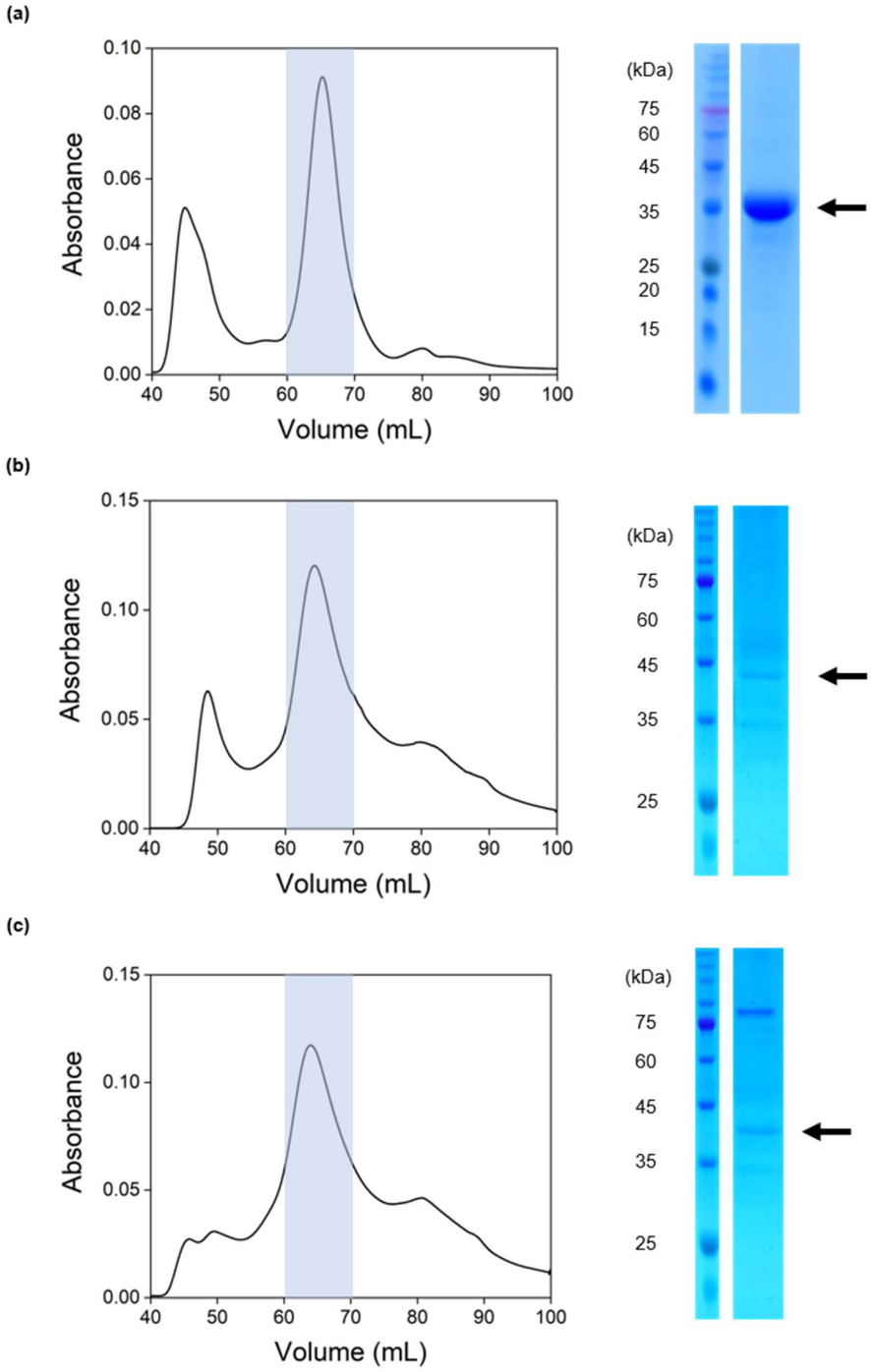

Figure 10. The size-exclusion chromatography of PmrF1-3 proteins. Representative FPLC traces and SDS-PAGE analysis of (a) PmrF1 (b) PmrF2 (c) PmrF3. In (c), a significant fraction of the protein was aggregated after size-exclusion chromatography, and the remaining soluble fraction was applied for SDS-PAGE. The arrows indicate the

size of the desired proteins.

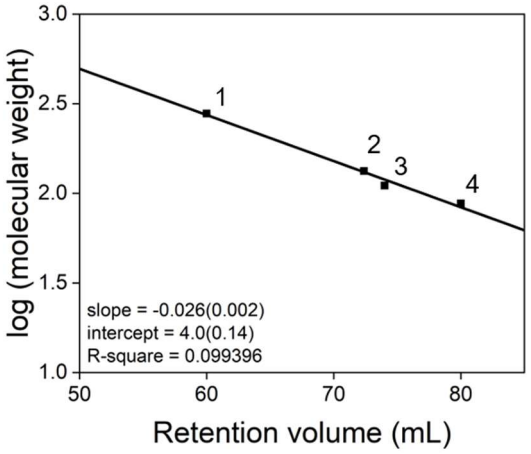

Figure 11. The calibration curve of size-exclusion chromatography to determine oligomeric state of PmrE and PmrF proteins. Proteins used for calibration are acetyltransferase from Bacillus anthracis (278.90 kDa), 2-keto-3-deoxyluconate aldolase from Sulfolobus solfataricus (133.36 kDa), DHRS6 from Homo sapiens (110.28 kDa), and phosphoheptose isomerase from Pseudomonas aeruginosa (87.68 kDa).

The retention time and elution volume of PmrE1–4 suggest that they are all tetramers (Figure 8 and Figure 11), indicating that they are different from hexameric UGDH from *Homo sapiens* (PDB 2Q3E) (43) and *Caenorhabditis elegans* (PDB 6OM8) (44) and dimeric UGDH from *Pyrobaculum islandicum DSM* 4184 (PDB 3VTF) (45), *Burkholderia cepacia* (PDB 2Y0E) (39), and *Klebsiella pneumonia* (PDB 3PID) (Figure 12 and Table 3). These results are consistent with the sequence analysis that PmrE1–4 proteins possess the protein-protein interactions (PPI) domain for dimerization but not hexamerization (Table 3 and Figure 13). PmrF1–3 were also identified to be tetramers, resembling the oligomeric states of GtrB (40). These data were also consistent with the presence of PPI domains for tetramerization in the sequence analysis (Figure 14).

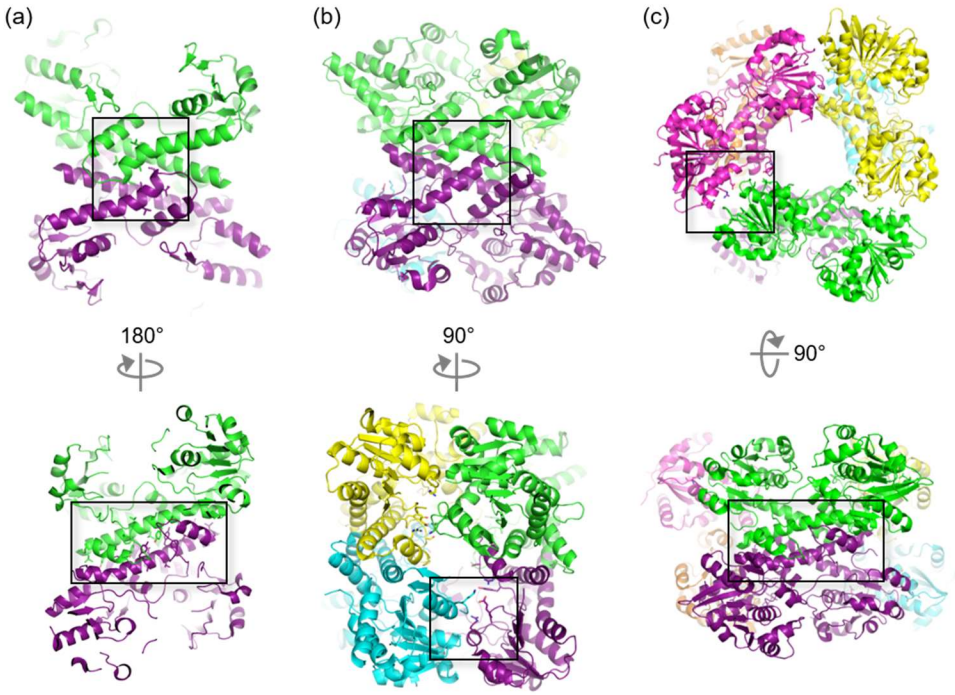

Figure 12. The structural analysis of PmrE-like proteins. Representative X-ray crystal structures of UGDH shown as (a) dimer (PDB 3PHL) (b) tetramer (PDB 3GG2) (c) hexamer (PDB 4RJT). The PPI domains are highlighted with black boxes.

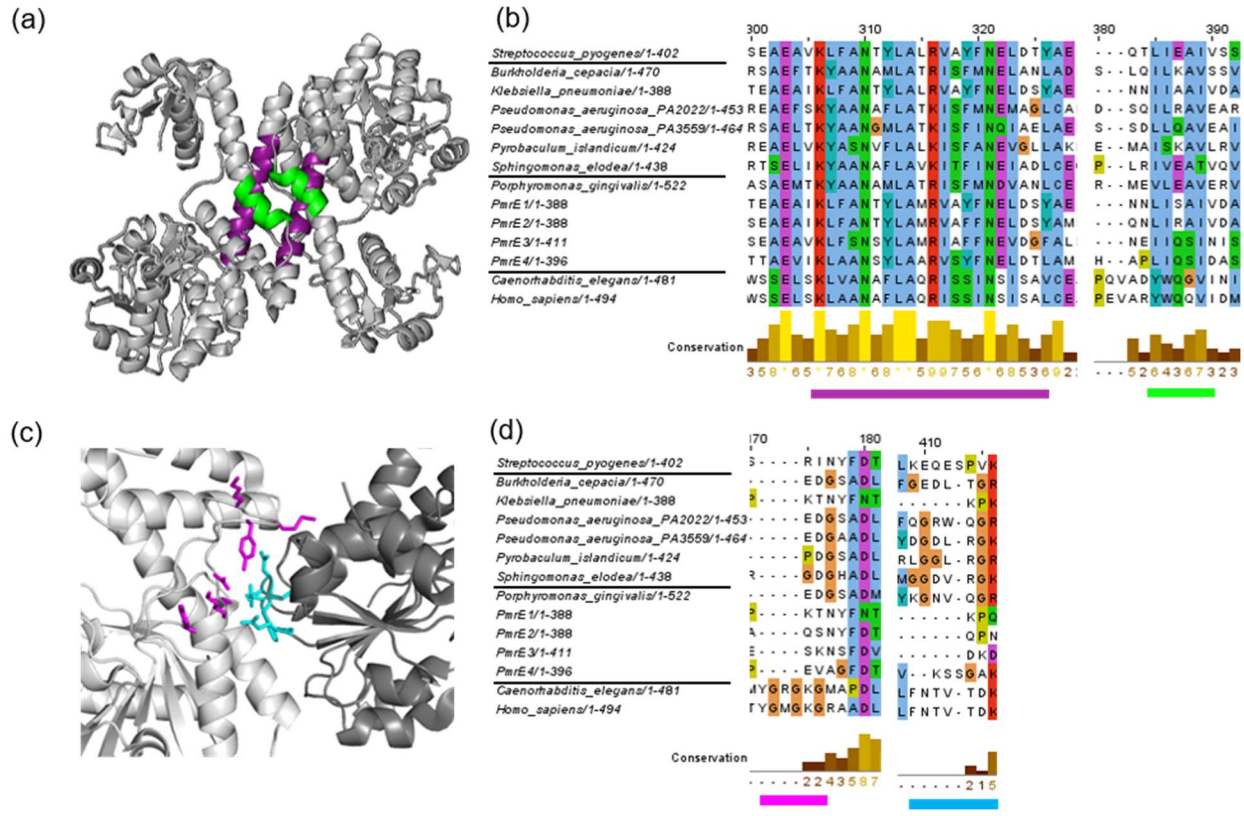

Figure 13. The structure and sequence analysis of PmrE-like proteins. (a) Two PPI domain for dimerization in Klebsiella pneumoniae UGDH (PDB 3PHL) colored in purple and green. (b) Multiple sequence alignment of UGDH, representing two PPI domains for dimerization, K(L|Y)(A|F)ANx(Y|F)LAx(R|K)(I|V)(S|A)(F|Y|S)(F|I)N-(E|S)(L|I|V)xx(L|Y) and (I|L)(I|L)xA (I|V) (c) The PPI domain for hexamerization shown in human UGDH (PDB 4RJT). The key residues are shown with magenta or cyan sticks. (d) Multiple sequence alignment of PPI domain of UGDHs that form hexamer.

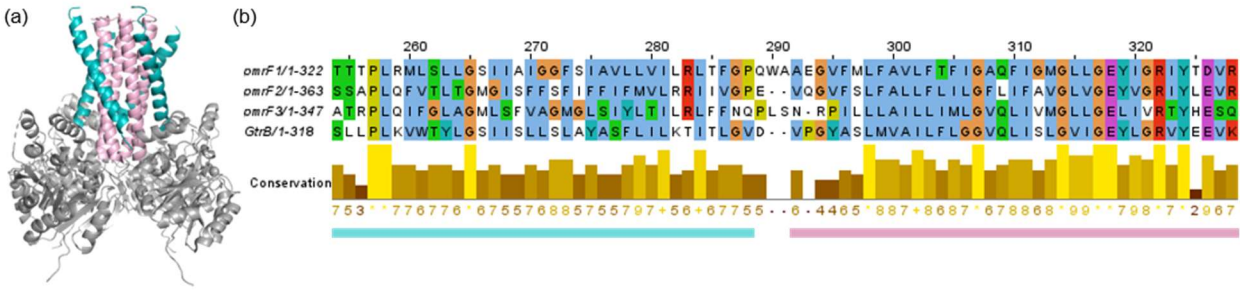

Figure 14. Structure and sequence analysis of pmrF genes. (a) The crystal structure of GtrB (PDB 5EKE). The transmembrane PPI domains are colored in cyan and light magenta. (b) Multiple sequence alignment of pmrF1–3 with GtrB, showing the PPI domains.

2.3. In vitro activities of the PmrE and PmrF proteins

The steady-state activity of PmrE1–4 was measured by altering the concentrations of NAD^+ or UDP-glucose and monitoring time-dependent absorption changes at 340 nm. Then, Michaelis–Menten kinetic parameters of PmrE1–4 were obtained from non-linear iterative analysis (Figure 15–16).

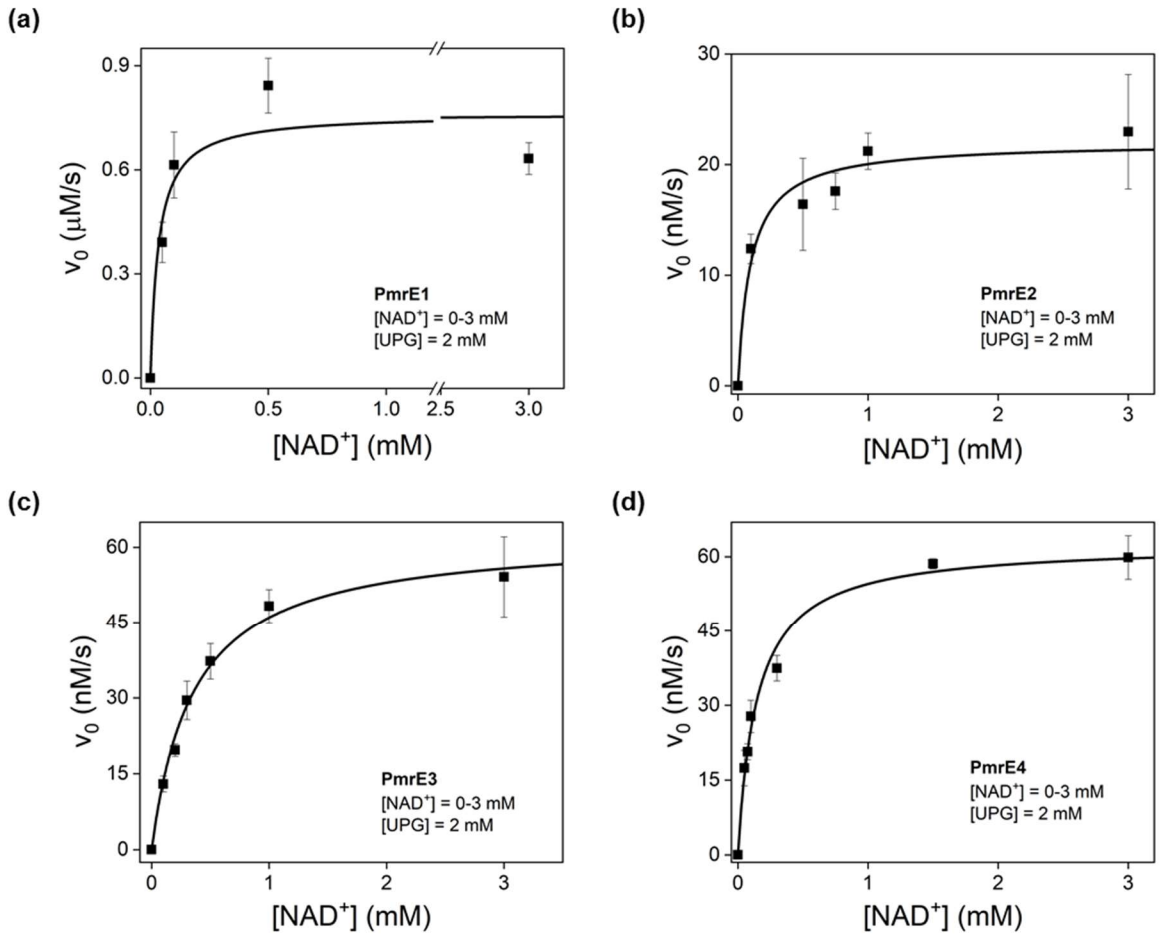

Figure 15. The steady-state kinetic analysis of PmrE1–4 with various concentrations of NAD^+. (a) PmrE1 (b) PmrE2 (c) PmrE3 (d) PmrE4.

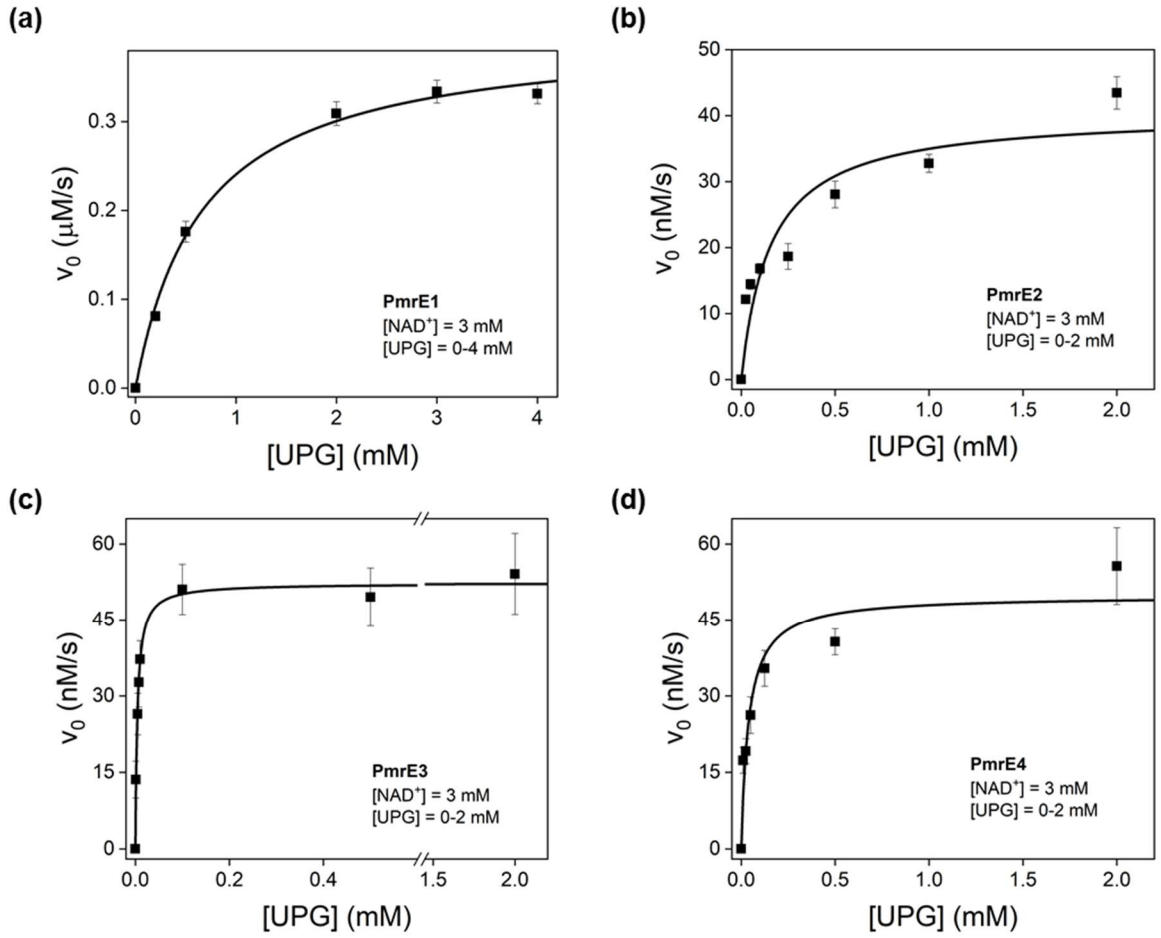

Figure 16. The steady-state kinetic analysis of PmrE1–4 with various concentrations of UPG. (a) PmrE1 (b) PmrE2 (c) PmrE3 (d) PmrE4.

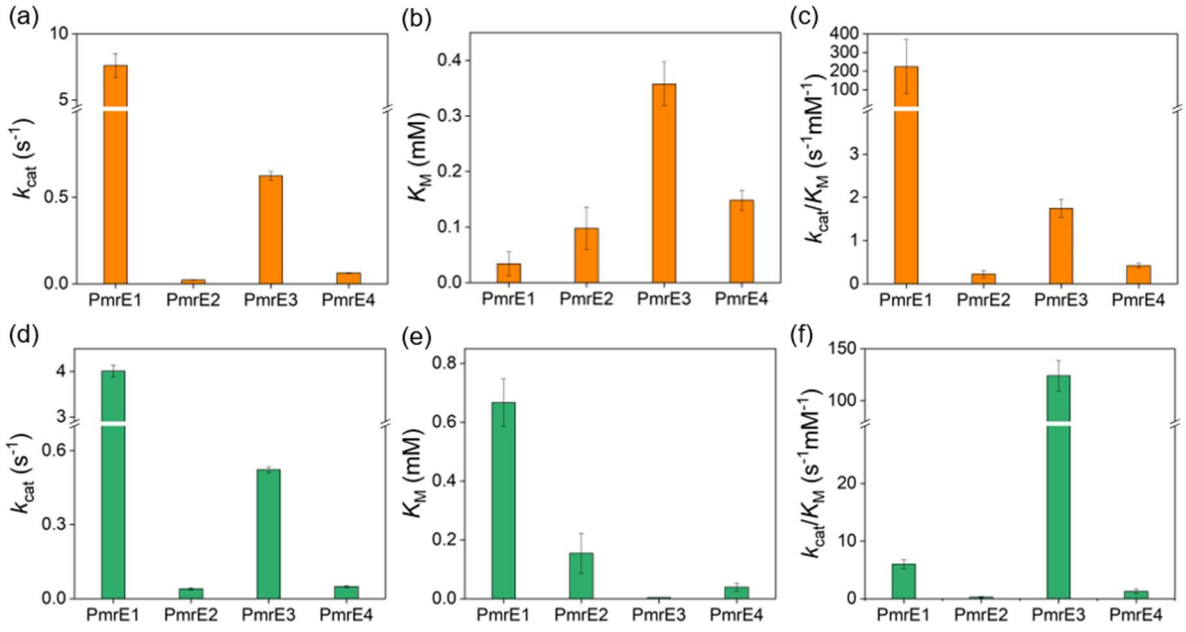

Figure 17. Michaelis–Menten kinetic parameters of PmrE1–4 proteins. The concentration of UPG (a–c) and NAD^+ (d–f) are fixed as 2 and 3 mM, respectively. (a, d) kcat, (b, e) KM, and (c, f) kcat/KM values.

All four PmrE proteins facilitated the reduction of NAD^+ to NADH in the presence of UDP–glucose (Figure 17A–C and Table 4A). Although all discovered PmrE proteins (PmrE2–4) exhibited considerably lower activity than PmrE1, they are kinetically competent in UDP–glucose oxidation coupled with NAD^+ reduction. They showed discrete kinetic parameters determined with NAD^+ (0–3 mM) and UDP–glucose (2 mM): PmrE1 >> PmrE3 > PmrE4 ≈ PmrE2 in turnover rates (k_{cat}) and catalytic efficiencies (k_{cat}/K_M) and PmrE3 > PmrE4 ≈ PmrE2 > PmrE1 in the Michaelis constant (K_M) for NAD^+. Notably, PmrE3 showed a substantially high K_M value, suggesting that it may show a weak binding affinity for NAD^+, and it could be related to sequence variations in one of the NAD^+–binding regions (I(A|S)(V|T)(G|P)T(P|D)) different from others.

The order of reactivities of PmrE proteins was similarly detected when UDP–glucose concentration was varied (0–2 mM) with a fixed concentration of NAD^+ (3 mM); PmrE1 >> PmrE3 > PmrE4 ≈ PmrE2 and PmrE3 >> PmrE1 > PmrE4 ≈ PmrE2, for k_{cat} and k_{cat}/K_M values, respectively, when K_M values for UDP–glucose were determined in the following order: PmrE1> PmrE2 > PmrE4 > PmrE3 (Figure 17D–F and Table 4B). Notably, PmrE3 exhibited substantially lower K_M and higher k_{cat}/K_M values than PmrE1

when PmrE1 showed relatively high K_M values. Because they possess highly conserved sequences that dictate UDP−glucose binding sites, dynamic motions that occur during the consumption of two substrates might determine their discrete reactivity. In addition, all Michaelis−Menten plots of PmrE1–4 displayed nearly hyperbolic curves (Figure 15–16), suggesting that two substrate−binding events occur non−cooperatively without significant allosteric transition. These results contrasted with hexameric UGDH (42, 44), suggesting that discrete oligomerization states, tetramer versus hexamer, determine the mode of interaction with two substrates.

The proposed mechanism of UGDHs suggests that two sequential hydride transfers from UDP−glucose to NAD^+ proceed via a nucleophilic cysteine residue (C253). The reaction was assisted by highly conserved residues, such as Y10, T118, K197, N201, K256, and D257 (the sequence numbers from UGDH in *Klebsiella pneumonia*) (39, 43, 46). These key residues were highly conserved in PmrE1–4, indicating that residues other than those in the active sites were responsible for their discrete catalytic activity. Nevertheless, the catalytic activities of PmrE2–4 demonstrated that they are kinetically competent UDP−glucose 6−dehydrogenases, and therefore, can be involved in lipid A modification for polymyxin resistance.

The activities of PmrF1–3 with UDP−glucose and UndP were determined by measuring UDP concentration converted from UDP−glucose as a surrogate substrate for UDP−L−Ara4FN. The concentration of UDP was calculated by calibration curve of luminescence intensity and UDP concentration (Figure 18). Only PmrF1 and PmrF2 showed glycosyltransferase activity, but not with PmrF3 (Figure 19), although they all possess sequence motifs that might be essential for substrate−binding. The lack of catalytic activity with PmrF3 might attribute to low protein stability because we observed that PmrF3 protein was aggregated during the assays and purification. Alternatively, unidentified residues critical for the reactivity may be absent in PmrF3. PmrF1 and PmrF2 yielded 99(23) and 146(30) nM of UDP, respectively, corresponding to 12 and 17% conversions of the added UndP (860 nM), respectively. The activity of PmrF1–2 are lower than those of GtrB reported previously (up to 200 nM product formation) (40), possibly because UDP−glucose is not the native substrate for PmrF. Nevertheless, the presence of the catalytic activities of PmrF1 and PmrF2 suggest that they can participate in lipid A modification, possibly leading to polymyxin resistance.

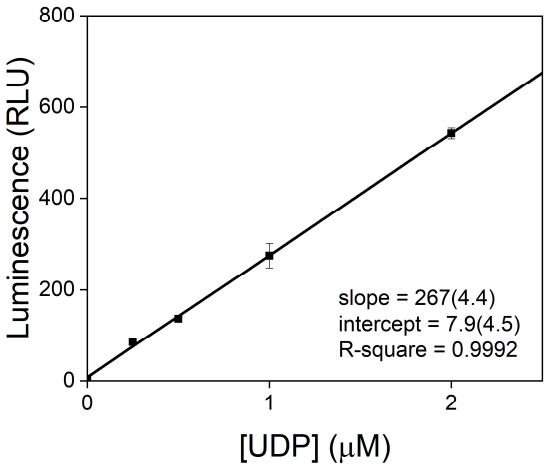

Figure 18. Standard curve of luminescence intensity versus UDP concentration.

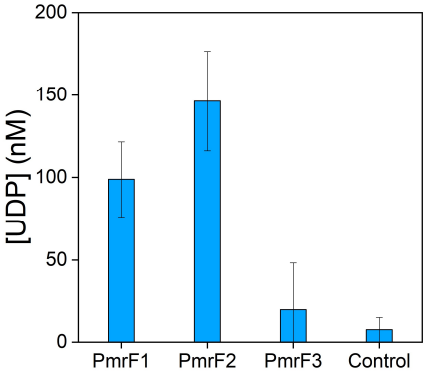

Figure 19. Glycosyltransferase activity of PmrF1, PmrF2 and PmrF3.The activity was measured with UndP (0.863 μM) and UPG (400 μM).

2.4. The minimal inhibitory concentrations of the discovered pmrE and pmrF genes

To monitor whether the catalytic activities of the *pmrE* and *pmrF* genes detected under *in vitro* conditions are related to the development of polymyxin resistance, we measured the minimal inhibitory concentrations (MICs). Two representative polymyxins, polymyxin B2 and E, were serially diluted in *E. coli* BL21 (DE3) cells expressing the putative *pmrE* genes (Figure 20A–B). No discernible MICs were observed in the cells against those with pET vector without any *pmrE* gene (shown as control), presumably because *pmrE* genes alone are incompetent in lipid A modification. Instead, a series of genes (Figure 1C) are necessary for polymyxin resistance.

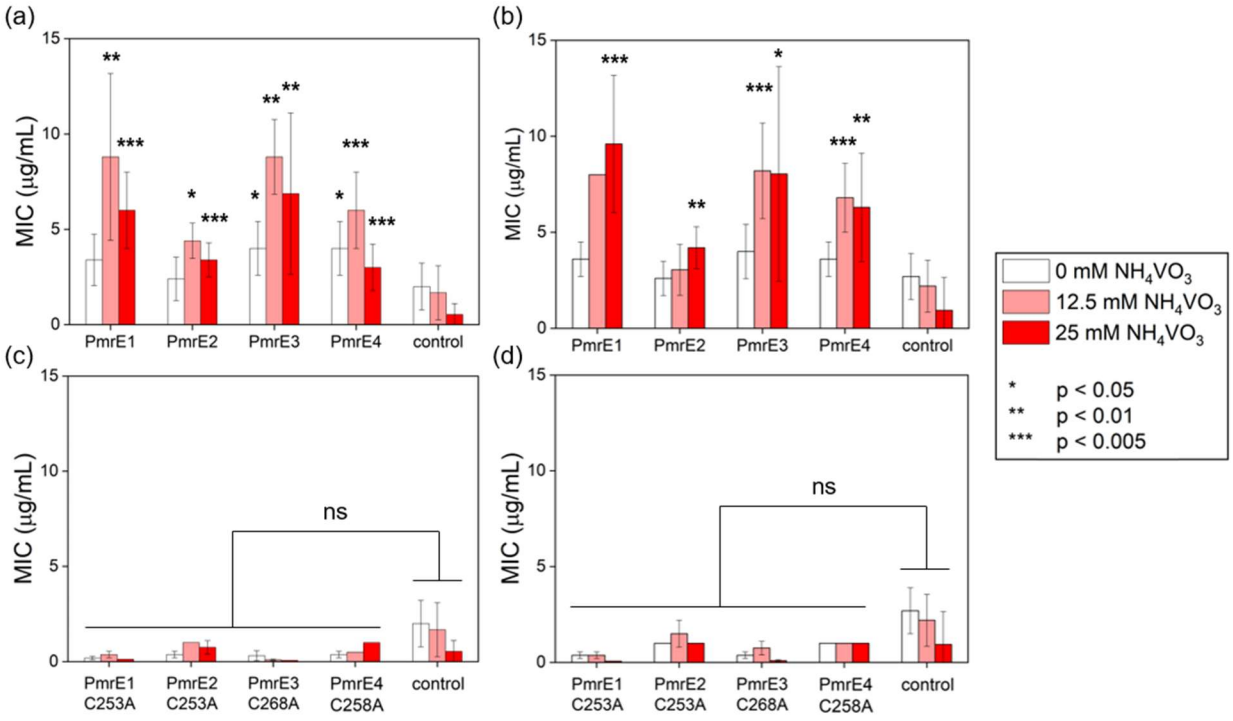

Figure 20. Minimal inhibitory concentration values of PmrE1–4 with polymyxin B2 and E upon different vanadate concentrations. PmrE1–4 with (a) polymyxin B2 and (b) polymyxin E. Catalytically inactive single variants with (c) polymyxin B2 and (d) polymyxin E. An empty vector of pET−28b(+) is applied as a control.

E. coli K12 possesses an *arn* operon associated with lipid A modification that is dormant under normal cell growth conditions. The introduction of environmental stimuli, such as low Mg^{2+} or Ca^{2+} concentrations, low pH, osmotic shock, and high concentrations of metal ions, including Fe^{3+}, Al^{3+}, and metavanadate (VO_3^-) (14, 15), can activate the gene cluster, resulting in lipid A modification. Therefore, we applied one of these conditions to stimulate the gene cluster of *E. coli* BL21(DE3) and detect any significant increase in MIC values due to the heterologous expression of discovered *pmrE* genes.

When we added 12.5 mM or 25 mM ammonium metavanadate (NH_4VO_3), the MIC values of cells overexpressing PmrE1–4 proteins were substantially elevated (Figure 20A–B). PmrE2–4 show higher MIC values than those of the control with 12.5 mM NH_4VO_3 for polymyxin B and 12.5–25 mM NH_4VO_3 for polymyxin E. Their MIC values roughly correlated with the kinetic parameters of PmrE1–4 measured under *in vitro* conditions (PmrE1 ≈ PmrE3 ≥ PmrE4 > PmrE2), indicating that polymyxin resistance emerged from the PmrE1–4 proteins.

To further validate the *in vivo* activities of PmrE proteins, we prepared single variants in which a catalytic cysteine residue was mutated to alanine (Figure 20C–D). The vanadate−dependent MIC values disappeared for all PmrE1–4 variants, indicating that the polymyxin resistance observed above was derived from the catalytic activities of PmrE1–4 in UDP−glucose oxidation, and the discovered *pmrE* genes contribute to polymyxin resistance.

We also measured the MIC values of BL21(DE3) pLysS cells expressing PmrF1–3 proteins (Figure 21A–B) with polymyxin B2 and E in the absence and presence of NH_4VO_3. The MIC values of PmrF1–2 were detected only in 25 mM NH_4VO_3 for both polymyxins but not PmrF3 regardless of NH_4VO_3 concentration. These results were consistent with the catalytic activities observed under *in vitro* conditions, indicating that *pmrF2* gene discovered from sediment microbiome can induce polymyxin resistance, but not *pmrF3*.

Upon mutation of the conserved acidic residue, which may correspond to D157 in GtrB in the sequence alignments (Figure 5C), into asparagine, the effective MIC values of PmrF1–2 disappeared (Figure 21C–D). These results indicate that the MIC values observed above were indeed derived from the reactivities of PmrF1–2. The data also suggest that the conserved aspartate residue plays a critical role in the transferase activity, similarly to D157 in GtrB, and is an essential sequence motif that dictates the chemical function of *pmrF* gene.

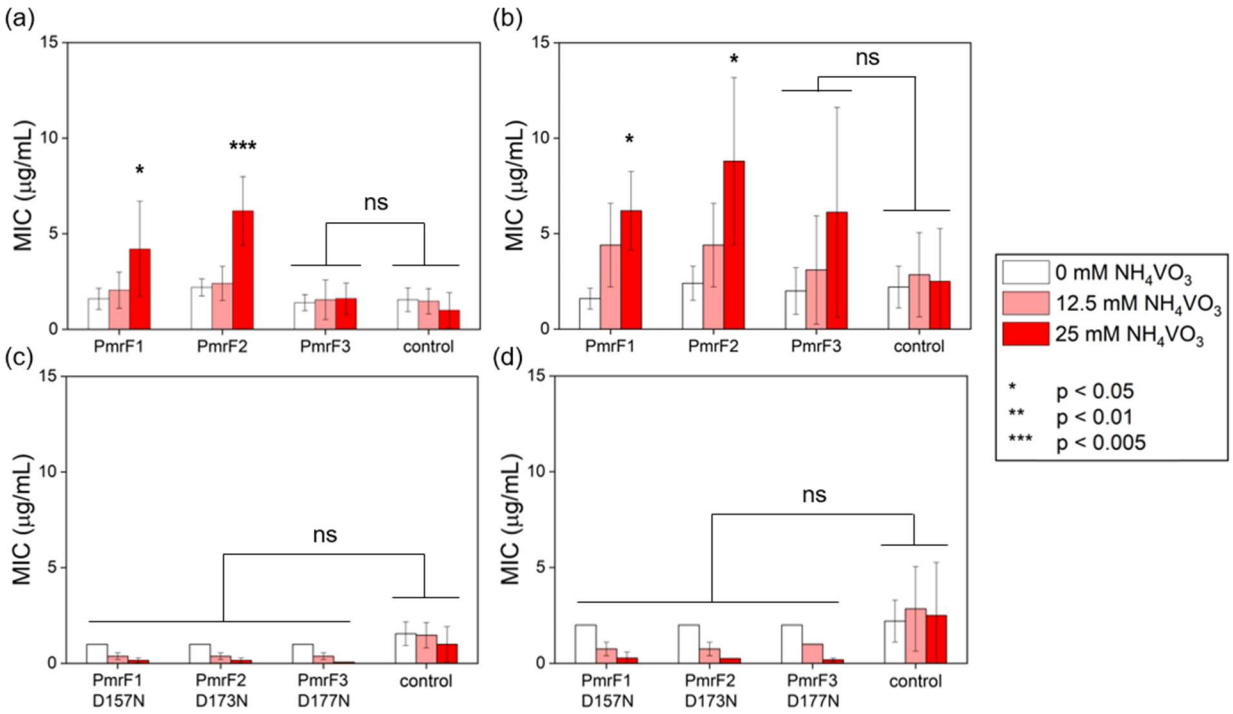

Figure 21. Minimal inhibitory concentration values of PmrF1–3 with polymyxin B2 and E upon different vanadate concentrations. PmrF1–3 with (a) polymyxin B2 and (b) polymyxin E. Catalytically inactive single variants with (c) polymyxin B2 and (d) polymyxin E. An empty vector of pET−21b(+) is applied as a control.

Chapter 3. Conclusion

We discovered and characterized *pmrE* and *pmrF* genes from metagenomes under *in vitro* and *in vivo* conditions and compared them with those from *E. coli*. Three *pmrE* (*pmrE*2–4) and one *pmrF* (*pmrF*2) genes displayed reactivity essential in lipid A modification, suggesting that their activities were directly related to the emergence of polymyxin resistance. In particular, whereas *pmrE* genes have been extensively investigated, the discovered *pmrE* genes are considerably dissimilar from others. In addition, we directed measured *in vitro* activities of *pmrF* genes, including the one from *E. coli*. Site-directed mutagenesis studies of *pmrF* genes also indicate that they require an acidic residue for transferase activity. This work demonstrated that *pmrE* and *pmrF* genes exhibit diverse sequence and function, expanding polymyxin resistomes.

Chapter 4. Materials and Methods

4.1. Data Collection

We have obtained 2,557 putative *pmr* genes from sediment samples using homology search against CARD database (40% ≤ sequence similarity < 80% and query coverage ≥ 70%). After clustering the sequences with a threshold of 40% sequence similarity, five non-redundant *pmr* genes were retained from each cluster that has more than five *pmr* genes (*pmrE*2–4 and *pmrF*2–3; Table 1). Additionally, two *pmr* genes (*pmrE*1 and *pmrF*1) were obtained from the CARD database as a reference.

4.2. Genome mining of putative PmrE proteins

Position-specific iterative BLAST (PSI-BLAST) (47) was performed in December 2021 on reference protein database and metagenomic protein database using four putative PmrE1–4 proteins with a cut-off value of 50% coverage and 25% sequence identity. Total 4004 proteins were used to generate a sequence-similarity network (SSN) using EFI-EST (http://efi.igb.illinois.edu/efi-est) (48). The resulting network was visualized in Cytoscape 3.8.1 using organic layout (Figure 2) (49).

4.3. Sequence and structure analysis

For structure-guided sequence analysis of PmrE-like proteins, we collected the sequences of nine UGDHs, of which X-ray crystal structures or oligomeric sizes were identified (Table 3). The sequence identity was obtained from the BLAST global alignments. Sequences included for alignments in figure 4 are as follows: *Streptococcus pyogenes* (UniProtKB P0C0F4), *Burkholderia cepacia* (C9E261), *Klebsiella pneumoniae* (A0A0J9WZA6), *Pseudomonas aeruginosa* PA2022 (GenBank™ accession number NP_250712), *Pseudomonas aeruginosa* PA3559 (NP_252249), *Pyrobaculum islandicum* (UniProtKB A1RUM9), *Sphingomonas elodea* (A4UTT2), *Porphyromonas gingivalis* (Q7MVC7), *Caenorhabditis elegans* (Q19905), and *Homo sapiens* (O60701). We conducted multiple sequence alignments using Clustal Omega (Figure 3–4) (50). The NAD^+ and UDP-glucose-binding motifs were defined by inspecting the residues that show direct contact with the bound substrates in the X-ray crystal structures and high degrees of conservation in the sequence alignments. To identify protein-protein interface (PPI) domains for dimer and hexamer formations, we inspected the X-ray crystal structures of UGDH from *Klebsiella pneumoniae* (PDB 3PLN) and *Homo sapiens* (PDB 4RJT), respectively. For structure-guided sequence analysis of PmrF-like proteins, GtrB (PDB 5EKP) structure was applied.

4.4. Genome mining of putative PmrF proteins

Position-specific iterative BLAST (PSI-BLAST) was performed in December 2021 on reference protein database and metagenomic protein database using three putative PmrF1–3 proteins and GtrB protein with a cut-off value of 50% coverage and 25% sequence identity. Total 3491 proteins were used to generate a sequence-similarity network (SSN) using EFI-EST (http://efi.igb.illinois.edu/efi-est).(48) The resulting network was visualized in Cytoscape 3.8.1 using organic layout (Figure 5A) (49). At least four groups (1–4) were identified, which includes PmrF1–3 and GtrB, individually. The number of sequences for each network that include PmrF1, PmrF2, PmrF3 and GtrB is 541, 572, 958 and 543, respectively. The genes included within each group were aligned using MAFFT 7.490 with an G-ins-i algorithm option (51). The alignment was used to generate sequence logos using WebLogo3 (Figure 5C and Figure 6) (52).

4.5. Expression and purification of PmrE proteins

We selected *pmrE*1, *pmrE*2, *pmrE*3, and *pmrE*4 as the target gene for biochemical characterization. Prior of gene synthesis, the codons of the DNA fragments were optimized for further *E. coli* expression (General Biosystems). The genes were cloned into pET28b(+)/kan^R vector using NdeI and Xho1 restriction enzyme sites and transformed to either DH5α or BL21(DE3) for sequencing or protein expression, respectively. All protein sequences were followed by a six-histidine tag at the N-terminus.

For the expression of target PmrE, picked a single colony of BL21(DE3) and inoculated in 10 mL autoclaved LB media containing 50 mg/L kanamycin. The cells were grown in 200 rpm orbital shaker at 37 °C for 18 h and inoculated in 1 L autoclaved LB media containing 50 mg/L kanamycin. At an optical density at 600 nm (OD_{600}) value of 0.7, the temperature was reduced to 15 °C and induced with 0.1 mM IPTG. After grown in 150 rpm orbital shaker for 18 h, the cells were harvested by centrifugation at 5000 rpm for 10 min at 4 °C and the cell pastes were frozen in liquid nitrogen and stored at –80 °C for further usage.

The cell pastes were resuspended in lysis buffer (25 mM Tris/HCl buffer, pH 8.0) and lysed by sonication for 30 min in an ice bath (on/off = 3 s each). After centrifugation at 13000 rpm for 30 min at 4 °C, the supernatants were loaded to a Ni affinity column (HisTrap FF column, GE Healthcare Life Sciences), pre-equilibrated with the lysate buffer at 4 °C by ÄKTA Protein Purification Systems. Applying elution buffer (25 mM Tris/HCl buffer, pH 8.0 with 500 mM imidazole) in a linear gradient (5–50%) eluted all proteins around ~100 mM imidazole condition (Figure 7). The relatively pure fractions (~80–90%) were determined by SDS-PAGE and concentrated using centrifugal concentrator with 10 *k*Da cutoff membrane filters. The purification step was followed by size exclusion chromatography (HiLoad® 16/600 Superdex® 200 pg) with the buffer of 25 mM Tris/HCl buffer, pH 8.0 with 150 mM NaCl (Figure 8).

The purified protein was concentrated up to ~10–100 μM and stored at –80 °C until further usage. The protein concentration was determined by UV–vis spectrophotometer (Agilent Cary 8454) using the absorption coefficients at 280 nm estimated from the sequence.

4.6. Expression and purification of PmrF proteins

We selected *pmrF*1, *pmrF*2, and *pmrF*3 as the target gene for biochemical characterization. Prior of gene synthesis, the codons of the DNA fragments were optimized for further *E. coli* expression (General Biosystems). The genes were cloned into pET21b(+)/amp^R vector using NheI and Xho1 restriction enzyme sites and transformed to either DH5α or C41 for sequencing or protein expression, respectively. All protein sequences were followed by a six−histidine tag at the N−terminus.

For the expression of target PmrF, picked a single colony of C41 and inoculated in 10 mL autoclaved LB media containing 100 mg/L ampicillin. The cells were grown in 200 rpm orbital shaker at 37 °C for 18 h and inoculated in 1 L autoclaved LB media containing 100 mg/L ampicillin. At an optical density at 600 nm (OD_{600}) value of 0.7, the temperature was reduced to 22 °C and induced with 0.5 mM IPTG. After grown in 150 rpm orbital shaker for 18 h, the cells were harvested by centrifugation at 5000 rpm for 10 min at 4 °C and the cell pastes were frozen in liquid nitrogen and stored at –80 °C for further usage.

The cell pastes were resuspended in lysis buffer (25 mM sodium HEPES buffer, pH 7.5 with 150 mM NaCl and 20 mM $MgSO_4$) and lysed by sonication for 30 min in an ice bath (on/off = 3 s each). After centrifugation at 13000 rpm for 30 min at 4 °C, the pellet was resuspended in extraction buffer (lysis buffer with 1% (w/v) DDM). Resuspended mixture was incubated at 100 rpm for 1 h at 15 °C. The mixtures were centrifuged at 13000 rpm for 30 min at 4 °C and the supernatants were loaded to a Ni affinity column (HisTrap FF column, GE Healthcare Life Sciences), pre−equilibrated with the extraction buffer at 4 °C by ÄKTA Protein Purification Systems. An elution buffer (extraction buffer with 500 mM imidazole) was applied in a linear gradient (5–50%), resulting in the elution of PmrF proteins (Figure 9). The relatively pure fractions (~80–90%) were determined by SDS−PAGE and concentrated using centrifugal concentrator with 10 *k*Da cutoff membrane filters. The purification step was followed by size exclusion chromatography (HiLoad® 16/600 Superdex® 200 pg) with 25 mM sodium HEPES buffer (pH 7.5) with 150 mM NaCl and 0.1% (w/v) DDM (Figure 10). The purified protein was concentrated up to ~10–100 μM and stored at –80 °C until further usage. The protein concentration was determined by UV–vis spectrophotometer (Agilent Cary 8454) using the absorption coefficients at 280 nm estimated from the sequence.

4.7. In vitro activity assay of pmrE

Two substrates, NAD^+ and UDP−glucose, were dissolved in water, and diluted with the buffer used for the assay. Various concentrations of the substrates, NAD^+ and UDP−glucose, were mixed with 1 μM protein in 400 μL of 50 mM Tris (pH 8.7) buffer with 1% (w/v) DTT. The initial rate was measured by detecting the concentrations of NADH formation by time−resolved absorption changes at 340 nm by UV–vis spectrophotometer (Agilent Cary 8454). Steady−state kinetic parameters of PmrE proteins were obtained by varying the concentrations of one of the substrates, either NAD^+ or UDP−glucose, when the other was fixed to be 3 mM or 2 mM, respectively. The kinetic parameters, k_{cat}, K_M, and k_{cat}/K_M, were determined from non−linear iteration curve fits to the Michaelis−Menten equation (Table 4 and Figure 15–17). All parameters were calculated from the average of triplicate repeats. Observed parameters were compared with parameters of various polymyxin−resistant bacteria (Table 5).

4.8. In vitro activity assay of pmrF

The biochemical function of PmrF proteins were determined by using the method of GtrB activity assay (40). In short, the *pmrF* genes were transformed into *E. coli* C41 competent cells. After cell growth, protein expression, the lysis of cell pellets (2 g), and centrifugation, as described above, the pellets were resuspended in 30 mL of 100 mM Tris/HCl pH 8.0 buffer and sonicated for 1 h in an ice bath. The resuspension (5 μL) were mixed with 250 μL of 100 mM Tris/HCl 10 mM $MgCl_2$ 1 mM EDTA pH 8.0 buffer and 400 μM UPG and 0.86 μM UndP at the final concentrations. The solution was incubated for 1 h at room temperature after mild sonication for mixing. Then, UDP-Glo™ glycosyltrasnferase assay kit (Promega) was used to measure the concentrations of UDP by luminescence. The standard curve of luminescence intensity versus UDP concentration was measured independently (Figure 18). Quantification of protein concentration was done by densitometry using SDS-PAGE gel. The activity values were calculated from the average of triplicate repeats.

4.9. Determination of MIC values

Minimal inhibitory concentration (MIC) values for BL21(DE3) cells containing *pmrE* genes and BL21(DE3) pLysS cells containing *pmrF* genes were measured following the previously reported procedures.(29) In short, the plasmids containing *pmrE* or *pmrF* genes were transformed into BL21(DE3) or BL21(DE3) pLysS cells, respectively. The cells were grown on the LB/agar plate containing 50 mg/L kanamycin or 100 mg/L ampicillin and 35 mg/L chloramphenicol overnight at 37 °C. The cell culture was diluted with 0.85% saline until the OD_{625} to be 0.1, followed by mixing the 100 μL aliquot with 18.9 mL Mueller Hinton broth. Polymyxin B2 and polymyxin E (0–128 μg/mL) were dissolved in deionized water and added. After incubating at 34 °C for overnight, optical cell density (OD_{625}) was measured with the microplate reader (BioTeK Synergy^{TM} H1) to determine the minimum inhibitory concentrations of the antibiotics (Figure 20–21). The average and error range of MIC values of PmrE and PmrF proteins were calculated from five−time repeats and the average and error range of MIC values of PmrE and PmrF mutants were calculated from triplicate repeats. Statistical analysis was performed using Student's *t* test. Observed MIC values were compared with MIC values of various polymyxin−resistant bacteria (Table 6).

Chapter 5. Bibliography

1. Rice LB. 2008. Federal funding for the study of antimicrobial resistance in nosocomial pathogens: no ESKAPE. J Infect Dis 197:1079–81.
2. Mulani MS, Kamble EE, Kumkar SN, Tawre MS, Pardesi KR. 2019. Emerging Strategies to Combat ESKAPE Pathogens in the Era of Antimicrobial Resistance: A Review. Front Microbiol 10:539–539.
3. Hamidian M, Nigro SJ. 2019. Emergence, molecular mechanisms and global spread of carbapenem–resistant Acinetobacter baumannii. Microb Genom 5.
4. CDC. 2019. Antibiotic resistance threats in the United States. U.S. Department of Health and Human Services, CDC, Atlanta, GA.
5. Levy SB. 1992. The antibiotic paradox: How miracle drugs are destroying the miracle. Springer Science+Business Media, LLC, Plenum US.
6. Spellberg B, Blaser M, Guidos RJ, Boucher HW, Bradley JS, Eisenstein BI, Gerding D, Lynfield R, Reller LB, Rex J, Schwartz D, Septimus E, Tenover FC, Gilbert DN. 2011. Combating antimicrobial resistance: policy recommendations to save lives. Clin Infect Dis 52 Suppl 5:S397–428.
7. Kaye KS, Pogue JM, Tran TB, Nation RL, Li J. 2016. Agents of Last Resort: Polymyxin Resistance. Infect Dis Clin North Am 30:391–414.
8. Brown P, Dawson MJ. 2017. Development of new polymyxin derivatives for multi–drug resistant Gram–negative infections. J Antibiot 70:386–394.
9. Yahav D, Farbman L, Leibovici L, Paul M. 2012. Colistin: new lessons on an old antibiotic. Clin Microbiol Infect 18:18–29.
10. Nang SC, Azad MAK, Velkov T, Zhou QT, Li J. 2021. Rescuing the Last–Line Polymyxins: Achievements and Challenges. Pharmacol Rev 73:679–728.
11. Shaheen M, Li J, Ross Avena C, Vederas John C, Jensen Susan E. 2011. Paenibacillus polymyxa PKB1 Produces Variants of Polymyxin B–Type Antibiotics. Chem Biol 18:1640–1648.
12. Velkov T, Thompson PE, Nation RL, Li J. 2010. Structure––activity relationships of polymyxin antibiotics. J Med Chem 53:1898–1916.
13. Schindler M, Osborn MJ. 1979. Interaction of divalent cations and polymyxin B with lipopolysaccharide. Biochemistry 18:4425–4430.
14. Raetz CRH, Reynolds CM, Trent MS, Bishop RE. 2007. Lipid A modification systems in gram–negative bacteria. Annu Rev Biochem 76:295–329.
15. Chen HD, Groisman EA. 2013. The biology of the PmrA/PmrB two–component system: the major regulator of lipopolysaccharide modifications. Annu Rev Microbiol 67:83–112.
16. Simpson BW, Trent MS. 2019. Pushing the envelope: LPS modifications and their consequences. Nat Rev Microbiol 17:403–416.
17. Benedict RG, Langlykke AF. 1947. Antibiotic activity of Bacillus polymyxa. J Bacteriol 54:24.
18. Wolinsky E, Hines JD. 1962. Neurotoxic and Nephrotoxic Effects of Colistin in Patients with Renal Disease. N Engl J Med 266:759–762.

19. Liu BT, Song FJ, Zou M, Hao ZH, Shan H. 2017. Emergence of Colistin Resistance Gene mcr-1 in Cronobacter sakazakii Producing NDM-9 and in Escherichia coli from the Same Animal. Antimicrob Agents Chemother 61.
20. Landman D, Bratu S, Alam M, Quale J. 2005. Citywide emergence of Pseudomonas aeruginosa strains with reduced susceptibility to polymyxin B. J Antimicrob Chemother 55:954-957.
21. Lu X, Hu Y, Luo M, Zhou H, Wang X, Du Y, Li Z, Xu J, Zhu B, Xu X, Kan B. 2017. MCR-1.6, a New MCR Variant Carried by an IncP Plasmid in a Colistin-Resistant Salmonella enterica Serovar Typhimurium Isolate from a Healthy Individual. Antimicrob Agents Chemother 61.
22. Baron S, Hadjadj L, Rolain JM, Olaitan AO. 2016. Molecular mechanisms of polymyxin resistance: knowns and unknowns. Int J Antimicrob Agents 48:583-591.
23. Cai Y, Chai D, Wang R, Liang B, Bai N. 2012. Colistin resistance of Acinetobacter baumannii: clinical reports, mechanisms and antimicrobial strategies. J Antimicrob Chemother 67:1607-1615.
24. Wright GD. 2007. The antibiotic resistome: the nexus of chemical and genetic diversity. Nat Rev Microbiol 5:175-186.
25. Larsson DGJ, Flach C-F. 2022. Antibiotic resistance in the environment. Nat Rev Microbiol 20:257-269.
26. Olaitan AO, Morand S, Rolain J-M. 2014. Mechanisms of polymyxin resistance: acquired and intrinsic resistance in bacteria. Front Microbiol 5.
27. Gunn JS, Miller SI. 1996. PhoP-PhoQ activates transcription of pmrAB, encoding a two-component regulatory system involved in Salmonella typhimurium antimicrobial peptide resistance. J Bacteriol 178:6857-6864.
28. Barrow K, Kwon DH. 2009. Alterations in Two-Component Regulatory Systems of *phoPQ* and *pmrAB* Are Associated with Polymyxin B Resistance in Clinical Isolates of *Pseudomonas aeruginosa*. Antimicrob Agents Chemother 53:5150-5154.
29. Shin JH, Eom H, Song WJ, Rho M. 2018. Integrative metagenomic and biochemical studies on rifamycin ADP-ribosyltransferases discovered in the sediment microbiome. Sci Rep 8:12143.
30. Rho M, Song WJ. 2020. Discovery of Novel Gene Functions by Chemistry-Guided Targeted Sequence Analysis. Biochemistry 59:10-11.
31. Imchen M, Moopantakath J, Kumavath R, Barh D, Tiwari S, Ghosh P, Azevedo V. 2020. Current Trends in Experimental and Computational Approaches to Combat Antimicrobial Resistance. Front Genet 11.
32. Chen YY, Ko TP, Chen WH, Lo LP, Lin CH, Wang AH. 2010. Conformational changes associated with cofactor/substrate binding of 6-phosphogluconate dehydrogenase from Escherichia coli and Klebsiella pneumoniae: Implications for enzyme mechanism. J Struct Biol 169:25-35.
33. Jiang SS, Lin TY, Wang WB, Liu MC, Hsueh PR, Liaw SJ. 2010. Characterization of UDP-glucose dehydrogenase and UDP-glucose pyrophosphorylase mutants of Proteus mirabilis: defectiveness in polymyxin B resistance, swarming, and

virulence. Antimicrob Agents Chemother 54:2000–9.
34. Chen YY, Ko TP, Lin CH, Chen WH, Wang AH. 2011. Conformational change upon product binding to Klebsiella pneumoniae UDP–glucose dehydrogenase: a possible inhibition mechanism for the key enzyme in polymyxin resistance. J Struct Biol 175:300–10.
35. Loutet SA, Bartholdson SJ, Govan JRW, Campopiano DJ, Valvano MA. 2009. Contributions of two UDP–glucose dehydrogenases to viability and polymyxin B resistance of Burkholderia cenocepacia. Microbiology 155:2029–2039.
36. Hung RJ, Chien HS, Lin RZ, Lin CT, Vatsyayan J, Peng HL, Chang HY. 2007. Comparative analysis of two UDP–glucose dehydrogenases in Pseudomonas aeruginosa PAO1. J Biol Chem 282:17738–48.
37. Yooseph S, Sutton G, Rusch DB, Halpern AL, Williamson SJ, Remington K, Eisen JA, Heidelberg KB, Manning G, Li W, Jaroszewski L, Cieplak P, Miller CS, Li H, Mashiyama ST, Joachimiak MP, van Belle C, Chandonia JM, Soergel DA, Zhai Y, Natarajan K, Lee S, Raphael BJ, Bafna V, Friedman R, Brenner SE, Godzik A, Eisenberg D, Dixon JE, Taylor SS, Strausberg RL, Frazier M, Venter JC. 2007. The Sorcerer II Global Ocean Sampling expedition: expanding the universe of protein families. PLoS Biol 5:e16.
38. Campbell RE, Mosimann SC, van De Rijn I, Tanner ME, Strynadka NC. 2000. The first structure of UDP–glucose dehydrogenase reveals the catalytic residues necessary for the two–fold oxidation. Biochemistry 39:7012–23.
39. Rocha J, Popescu AO, Borges P, Mil–Homens D, Moreira LM, Sá–Correia I, Fialho AM, Frazão C. 2011. Structure of *Burkholderia cepacia* UDP–Glucose Dehydrogenase (UGD) BceC and Role of Tyr10 in Final Hydrolysis of UGD Thioester Intermediate. J Bacteriol 193:3978–3987.
40. Ardiccioni C, Clarke OB, Tomasek D, Issa HA, von Alpen DC, Pond HL, Banerjee S, Rajashankar KR, Liu Q, Guan Z, Li C, Kloss B, Bruni R, Kloppmann E, Rost B, Manzini MC, Shapiro L, Mancia F. 2016. Structure of the polyisoprenyl–phosphate glycosyltransferase GtrB and insights into the mechanism of catalysis. Nat Commun 7:10175.
41. Gandini R, Reichenbach T, Tan T–C, Divne C. 2017. Structural basis for dolichylphosphate mannose biosynthesis. Nat Commun 8:120.
42. Sennett NC, Kadirvelraj R, Wood ZA. 2012. Cofactor Binding Triggers a Molecular Switch To Allosterically Activate Human UDP–α–d–glucose 6–Dehydrogenase. Biochemistry 51:9364–9374.
43. Egger S, Chaikuad A, Kavanagh KL, Oppermann U, Nidetzky B. 2011. Structure and Mechanism of Human UDP–glucose 6–Dehydrogenase. J Biol Chem 286:23877–23887.
44. Beattie NR, Keul ND, Hicks Sirmans TN, McDonald WE, Talmadge TM, Taujale R, Kannan N, Wood ZA. 2019. Conservation of Atypical Allostery in C. elegans UDP–Glucose Dehydrogenase. ACS Omega 4:16318–16329.
45. Sakuraba H, Kawai T, Yoneda K, Ohshima T. 2012. Structure of a UDP–glucose dehydrogenase from the hyperthermophilic archaeon Pyrobaculum islandicum.

Acta Crystallogr F68:1003-1007.
46. Ge X, Penney LC, van de Rijn I, Tanner ME. 2004. Active site residues and mechanism of UDP-glucose dehydrogenase. Eur J Biochem 271:14-22.
47. Altschul SF, Madden TL, Schäffer AA, Zhang J, Zhang Z, Miller W, Lipman DJ. 1997. Gapped BLAST and PSI-BLAST: a new generation of protein database search programs. Nucleic Acids Res 25:3389-3402.
48. Zallot R, Oberg N, Gerlt JA. 2019. The EFI Web Resource for Genomic Enzymology Tools: Leveraging Protein, Genome, and Metagenome Databases to Discover Novel Enzymes and Metabolic Pathways. Biochemistry 58:4169-4182.
49. Shannon P, Markiel A, Ozier O, Baliga NS, Wang JT, Ramage D, Amin N, Schwikowski B, Ideker T. 2003. Cytoscape: a software environment for integrated models of biomolecular interaction networks. Genome Res 13:2498-504.
50. Sievers F, Wilm A, Dineen D, Gibson TJ, Karplus K, Li W, Lopez R, McWilliam H, Remmert M, Söding J, Thompson JD, Higgins DG. 2011. Fast, scalable generation of high-quality protein multiple sequence alignments using Clustal Omega. Mol Syst Biol 7:539.
51. Rozewicki J, Li S, Amada KM, Standley DM, Katoh K. 2019. MAFFT-DASH: integrated protein sequence and structural alignment. Nucleic Acids Res 47:W5-W10.
52. Crooks GE, Hon G, Chandonia JM, Brenner SE. 2004. WebLogo: a sequence logo generator. Genome Res 14:1188-90.
53. Campbell RE, Sala RF, van de Rijn I, Tanner ME. 1997. Properties and Kinetic Analysis of UDP-glucose Dehydrogenase from Group A Streptococci: IRREVERSIBLE INHIBITION BY UDP-CHLOROACETOL*. J Biol Chem 272:3416-3422.
54. Sieberth V, Rigg GP, Roberts IS, Jann K. 1995. Expression and characterization of UDPGlc dehydrogenase (KfiD), which is encoded in the type-specific region 2 of the Escherichia coli K5 capsule genes. J Bacteriol 177:4562-5.
55. Barbas A, Popescu A, Frazão C, Arraiano CM, Fialho AM. 2013. Rossmann-fold motifs can confer multiple functions to metabolic enzymes: RNA binding and ribonuclease activity of a UDP-glucose dehydrogenase. Biochem Biophys Res Commun 430:218-24.
56. Riegert AS, Raushel FM. 2021. Functional and Structural Characterization of the UDP-Glucose Dehydrogenase Involved in Capsular Polysaccharide Biosynthesis from Campylobacter jejuni. Biochemistry 60:725-734.
57. Kadirvelraj R, Custer GS, Keul ND, Sennett NC, Sidlo AM, Walsh RM, Wood ZA. 2014. Hysteresis in Human UDP-Glucose Dehydrogenase Is Due to a Restrained Hexameric Structure That Favors Feedback Inhibition. Biochemistry 53:8043-8051.
58. Kandiba L, Eichler J. 2016. AglM and VNG1048G, Two Haloarchaeal UDP-Glucose Dehydrogenases, Show Different Salt-Related Behaviors. Life (Basel) 6.

59. Granja AT, Popescu A, Marques AR, Sá-Correia I, Fialho AM. 2007. Biochemical characterization and phylogenetic analysis of UDP-glucose dehydrogenase from the gellan gum producer Sphingomonas elodea ATCC 31461. Appl Microbiol Biotechnol 76:1319-27.
60. Wu MM, Huang HD, Li GQ, Zhou JF, Ma T. 2015. Biochemical characterization and functional analysis of UDP-glucose dehydrogenase, in the synthesis of biopolymer Ss from Sphingomonas sanxanigenens NX02. Prikl Biokhim Mikrobiol 51:30-6.
61. Li J, Rayner CR, Nation RL, Owen RJ, Spelman D, Tan KE, Liolios L. 2006. Heteroresistance to colistin in multidrug-resistant Acinetobacter baumannii. Antimicrob Agents Chemother 50:2946-50.
62. Zheng B, Dong H, Xu H, Lv J, Zhang J, Jiang X, Du Y, Xiao Y, Li L. 2016. Coexistence of MCR-1 and NDM-1 in Clinical Escherichia coli Isolates. Clin Infect Dis 63:1393-1395.
63. Chew KL, La MV, Lin RTP, Teo JWP. 2017. Colistin and Polymyxin B Susceptibility Testing for Carbapenem-Resistant and mcr-Positive Enterobacteriaceae: Comparison of Sensititre, MicroScan, Vitek 2, and Etest with Broth Microdilution. J Clin Microbiol 55:2609-2616.
64. Zeng KJ, Doi Y, Patil S, Huang X, Tian GB. 2016. Emergence of the Plasmid-Mediated mcr-1 Gene in Colistin-Resistant Enterobacter aerogenes and Enterobacter cloacae. Antimicrob Agents Chemother 60:3862-3.
65. Malott RJ, Steen-Kinnaird BR, Lee TD, Speert DP. 2012. Identification of hopanoid biosynthesis genes involved in polymyxin resistance in Burkholderia multivorans. Antimicrob Agents Chemother 56:464-71.
66. Lin QY, Tsai YL, Liu MC, Lin WC, Hsueh PR, Liaw SJ. 2014. Serratia marcescens arn, a PhoP-regulated locus necessary for polymyxin B resistance. Antimicrob Agents Chemother 58:5181-90.

Chapter 6. Tables

Table 1. The protein sequences studied in this work. (a) PmrE1–4 (b) PmrF1–3
(a)

Protein	Sequence
PmrE1	MKITISGTGYVGLSNGLLIAQNHEVVALDILPSRVAMLNDRISPIVDKEIQQFLQSDKIHFNATLDK NEAYRDADYVIIATPTDYDPKTNYFNTSSVESVIKDVVEINPYAVMVIKSTVPVGFTAAMHKKYR TENIIFSPEFLREGKALYDNLHPSRIVIGERSERAERFAALLQEGAIKQNIPMLFTDSTEAEAIKLFA NTYLAMRVAYFNELDSYAESLGLNSRQIIEGVCLDPRIGNHYNNPSFGYGGYCLPKDTKQLLANY QSVPNNLISAIVDANRTRKDFIADAILSRKPQVVGIYRLIMKSGSDNFRASSIQGIMKRIKAKGVE VIIYEPVMKEDSFFNSRLERDLATFKQQADVIISNRMAEELKDVADKVYTRDLFGSD
PmrE2	MKITVAGLGYVGLSNAVLLAQNHTVTAIDISQDRVDQVNAKTSPIVDADIEDFLANHTLDLTATT DAEAAYKDADFIIVATPTNYDAQSNYFDTSSVETVINHALKANPNATIIVKSTIPVGFIDGIRTQMN SQNIVFSPEFLREGRALYDNLHPSRIIVGAQTEAAKTFANLLIEGAITKDVLVQFTDASEAEAIKLF ANTYLAMRVAFFNELDSYAMSRGMDSRQIINGISLDPRIGNHYNNPSFGYGGYCLPKDTKQLLA NYSEVPQNLIRAIVDANRTRKDFLSDRIIAMQPNIVGVHRLVMKAGSDNFRQSSIQGIMKRVKAK GIEVIVYEPELQETEFFNSRVITDLEAFKAEADVIVANRITDDLRDVAAKVFSRDLFGAD
PmrE3	MKQLGINEMNPGLPKQICIIGAGYVGMSYAVLISSFADIKIWDIDSKKRDLINAKKLPIQDLDSESI LSEKENWNIVASKNLNEALNKSQLVLICISTDFNESKNSFDVNEMNNLIDQVRKYSPNVQIVIKST VPIGYSAKITQETGLNILFSPEFLREGMAIRDNQFPSRIIIGKTNQNQACDPYLSVAKEIAKNSPEIFE MSASEAEAVKLFSNSYLAMRIAFFNEVDGFALKNNLLIKDIIEGMSADNRIGNYYNNPSFGFGGY CLPKDSRQALVSMNDLPNEIIQSINISNSKRKEFISKYLLHMDKDLYGFYRINMKENSDNMRESAS IEIIKILLSAGKQVIIYEPLLNNTNDFDNFELVKNLDEFKERSDIIIANRVTEEILDCKEKLFSRDLSY DTKIRPKNI
PmrE4	MLNKKVLVFGAGYVGFSLSVVMARAANVTVVDIRPDIIRSINAGRSPIEDLDIDKHLMIGLSSNRL NAQLYSQKLIEEADFVVLALPTSFNPEVAGFDTSALDDVIAKVADIDKSKPIIIKSTIPVGYTQKIIE KFGLSECYYSPEFLREGRATYDNLNPSRIVIGSTSTHAKEFVKILDDASHQRNTKKVFTDNTTAEV IKLAANSYLAARVSYFNELDTLAMIAGLNAVQLIDGVCADPRIGDGYNNPSFGYGGYCLPKDVK QFQRSFLDFKIHAPLIQSIDASNQQRIVEIINFVKSSGAKNIGIYRAQMKQGSDNARDSVNLAVLSQ LSAMPTLRVKIFEPKIDLPENLSTFKVNEFETFCDWSDLILANRDAVELREYHYKVLTRDIYNEN

(b)

Protein	Sequence
PmrF1	MFEIHPVKKVSVVIPVYNEQESLPELIRRTTTACESLGKEYEILLIDDGSSDNSAHMLVEASQAENS HIVSILLNRNYGQHSAIMAGFSHVTGDLIITLDADLQNPPEEIPRLVAKADEGYDVVGTVRQNRQ DSWFRKTASKMINRLIQRTTGKAMGDYGCMLRAYRRHIVDAMLHCHERSTFIPILANIFARRAIEI PVHHAEREFGESKYSFMRLINLMYDLVTCLTTTPLRMLSLLGSIIAIGGFSIAVLLVILRLTFGPQWA AEGVFMLFAVLFTFIGAQFIGMGLLGEYIGRIYTDVRARPRYFVQQVIRPSSKENE
PmrF2	MISYLSSVIIAQLQNPQVKNTMLDLSVIIPIYNEQDSIPELYQRTHETLEKLGRSYEIIFVNDGSADK SAILLDELHEQDSQHVKVIHFNGNFGQHMAIMAGFENSTGLAVVTLDADLQNPPEEIPKLITAMD EGHDIVEGMRQARKDNAFRRYASRLNNWIRHKTTGIRLKDQGSMLRAYNRRVVELMVLSKERA TYIPALAYSYASNPGFVEVNHAERAHGESKYSLFRLLRLHFDLMAGFSSAPLQFVTLTGMGISFFS FIFFIFMVLRRIIVGPEVQGVFSLFALLFLILGFLIFAVGLVGEYVGRIYLEVRNRPRFVIRKILEPSKI TAAKTPKTKQEKQINTKKAEKPGEESPPKTE
PmrF3	MSDGMMDLTNFHPETDVFAPIQTTNKVDVSVVIPVFNEDESIPELHNRLTTSLLSTGKNYEIIYIDD GSTDGSFEKLKSIQYQDSRVWIIQLRRNFGQAAAFSAGFDLAHGEVIVTLDGDLQNDPADIPNLL EKLDEGFDVVSGWRVNRKDQFLTRRVPSILANAMISRVTGLELHDYGCSLKAYRQEVVKNIKLY GELHRFIPAIASWMGIKVAEIPVNHAPRKHGRSHYGLGRTLKVFLDLITVKFLLNYATRPLQIFGL AGMLSFVAGMGLSIYLTILRLFFNQPLSNRPILLLAILLIMLGVQLIVMGLLGELIVRTYHESQGKSI YVVRNVLHSPDGSKQES

Table 2. Sequence identity value compared to each other sequence for (a) PmrE1−4 and (b) PmrF1−3. All sequence identity values were calculated by BLASTp.

(a)

	PmrE1	PmrE2	PmrE3	PmrE4
PmrE1	-	64%	39%	41%
PmrE2	-	-	39%	39%
PmrE3	-	-	-	34%
PmrE4	-	-	-	-

(b)

	PmrF1	PmrF2	PmrF3
PmrF1	-	41%	40%
PmrF2	-	-	34%
PmrF3	-	-	-

Table 3. The oligomeric state of various UGDH proteins.

Oligomeric State	PDB code	Organism (UniprotKB ID)	Reference
Monomer	-	*Streptococcus pyogenes* (P0C0F4)	(53)
Dimer	2Y0E	*Burkholderia cepacia* (C9E261)	(39)
	-	*Escherichia coli* K-5	(54)
	3PLN	*Klebsiella pneumonia* (A0A0J9WZA6)	(34)
	-	*Pseudomonas aeruginosa* (NP_250712/252249)	(36)
	3VTF	*Pyrobaculum islandicum* (A1RUM9)	(45)
	4A7P	*Sphingomonas elodea* (A4UTT2)	(55)
	7KWS	*Campylobacter jejuni NCTC 11168*	(56)
Tetramer	3GG2	*Porphyromonas gingivalis* (Q7MVC7)	Unpublished[§]
	-	*Escherichia coli* (PmrE1)	This work
	-	Metagenome (PmrE2)	This work
	-	Metagenome (PmrE3)	This work
	-	Metagenome(PmrE4)	This work
Hexamer	2O3J	*Caenorhabditis elegans* (Q19905)	unpublished[§]
	2Q3E/4RJT	*Homo sapiens* (O60701)	(43, 57)
Dodecamer	-	*Halobacterium salinarum*	(58)
	-	*Haloferax volcanii*	(58)

[§]The biological assembly was assigned by authors and generated by PISA (software).

Table 4. The Michaelis–Menten kinetic parameters of PmrE1–4. The steady-state catalytic activities were determined with (a) 2 mM UDP-glucose and (b) 3 mM NAD^+.

(a)

	k_{cat} (s^{-1})	K_M (μM)	k_{cat}/K_M (s^{-1} μM^{-1})
PmrE1	7.6(0.9)	34(22)	2.2(1.5) x 10^{-1}
PmrE2	2.2(0.1) x 10^{-2}	98(38)	2.2(0.9) x 10^{-4}
PmrE3	6.2(0.2) x 10^{-1}	3.6(0.4) x 10^{2}	1.7(0.2) x 10^{-3}
PmrE4	6.3(0.2) x 10^{-2}	1.5(0.2) x 10^{2}	4.2(0.5) x 10^{-4}

(b)

	k_{cat} (s^{-1})	K_M (μM)	k_{cat}/K_M (s^{-1} μM^{-1})
PmrE1	4.0(0.1)	6.7(0.8) x 10^{2}	6.0(0.7) x 10^{-3}
PmrE2	4.0(0.5) x 10^{-2}	1.5(0.7) x 10^{2}	2.6(1.1) x 10^{-4}
PmrE3	5.2(0.1) x 10^{-1}	4.2(0.5)	1.2(0.1) x 10^{-1}
PmrE4	5.0(0.4) x 10^{-2}	39(13)	1.3(0.4) x 10^{-3}

Table 5. Kinetic parameters of various PmrE from different organisms for various concentrations of (a) NAD^+ (b) UDP−glucose. The assays were conducted with 50–100 mM Tris/HCl (pH 8.7) buffer with minor alterations as noted in the last column.

(a) NAD^+ with 2 mM UDP−glucose

Organism	k_{cat} (s^{-1})	K_M (mM)	k_{cat}/K_M ($mM^{-1}s^{-1}$)	Ref	Condition
Streptococcus pyogenes	1.8(0.1)	0.065(0.006)	27(3)	(46)	2 mM DTT
Burkholderia cepacia	6.7	0.53	12	(39)	10 mM $MgCl_2$
Klebsiella pneumoniae	0.037(0.003)	0.11(0.01)	0.066(0.006)	(32)	1 mM DTT
Sphingomonas elodea	7.63	0.4	19	(59)	5 mM DTT/ 10 mM $MgCl_2$
Sphingomonas sanxanigenens	0.84	0.38	2.2	(60)	5 mM DTT/ 10 mM $MgCl_2$
Escherichia coli (PmrE1)	7.6(0.9)	0.034(0.022)	2.2(1.4) x 10^2	This work	1 mM DTT
Metagenome (PmrE2)	2.2(0.1) x 10^{-2}	0.098(0.038)	0.22(0.09)		
Metagenome (PmrE3)	6.2(0.2) x 10^{-1}	0.36(0.04)	1.7(0.2)		
Metagenome (PmrE4)	6.3(0.2) x 10^{-2}	0.15(0.02)	0.42(0.05)		

ND: Not determined

(b) UDP−glucose with 3 mM NAD^+

Organism	k_{cat} (s^{-1})	K_M (mM)	k_{cat}/K_M (mM^{-1} s^{-1})	Ref	Condition
Streptococcus pyogenes	1.8(0.1)	2.0(0.4) x 10^{-2}	90(17)	(46)	2 mM DTT
Burkholderia cepacia	6.9	0.23	30	(39)	10 mM $MgCl_2$
Klebsiella pneumoniae	0.037(0.003)	0.67(0.03)	0.011(0.001)	(32)	1 mM DTT
Sphingomonas elodea	8.7	0.87	10	(59)	5 mM DTT/ 10 mM $MgCl_2$
Sphingomonas sanxanigenens	0.97	0.47	2.1	(60)	5 mM DTT/ 10 mM $MgCl_2$
Escherichia coli (PmrE1)	4.0(0.1)	0.67(008)	6.0(0.7)	This work	1 mM DTT
Metagenome (PmrE2)	4.0(0.5) x 10^{-2}	0.15(0.07)	0.26(0.12)		
Metagenome (PmrE3)	5.2(0.1) x 10^{-1}	4.2(0.5) x 10^{-3}	12(1) x 10^2		
Metagenome (PmrE4)	5.0(0.4) x 10^{-2}	0.039(0.013)	1.3(0.4)		

Table 6. The MIC values of polymyxin-resistant bacteria.

Organism	MIC (μg/mL)		Reference
	Polymyxin B	Polymyxin E (colistin)	
Acinetobacter baumannii	ND	3–10	(61)
Salmonella enterica YL14P053	ND	4	(21)
Cronobacter sakazakii WF5-21C	ND	4	(19)
Pseudomonas aeruginosa	0.5–8	ND	(20)
Escherichia coli EC1002	4	4	(62)
Escherichia coli (PmrE1)	>4*	8*	This work
Metagenome (PmrE2)	>2*	>4*	This work
Metagenome (PmrE3)	>4*	>8*	This work
Metagenome (PmrE4)	>4*	>4*	This work
Escherichia coli (PmrF1)	>2*	>4*	This work
Metagenome (PmrF2)	>4*	>4*	This work
Enterobacter aerogenes	8	4	This work
Enterobacter cloacae GB38	>32	>32	(63)
Burkholderia multivorans ATCC 17616	256	512	(64)
Serratia marcescens 3927	2,048	ND	(65)
Acinetobacter baumannii	ND	3–10	(66)

ND: Not determined

*Measured in the presence of 25 mM NH_4VO_3

Abstract in Korean

현재 그람음성 세균에 대한 항생제의 필요성이 증대되고 있으며 폴리마이신은 그람음성 세균에 대한 항생제의 마지막 대응방안으로 여겨진다. 따라서 세균성 질병의 진단, 항생제 투여 및 신약 개발에 있어 폴리마이신 내성 유전자의 발견과 생화학적 성질의 분석이 시급한 과제로 떠올랐다. 본 연구에서는 해양미생물균주에서 기존에 알려지지 않았던 pmrE 와 pmrF 에 속하는 새로운 폴리마이신 내성 유전자를 찾아내었다. 새로운 유전자와 기존에 보고된 유전자들 사이의 서열의 유사도는 낮게 나타난다. 하지만 새로운 유전자에서 발현된 단백질이 폴리마이신 내성 기작 중 pmrE 와 pmrF 유전자가 관여하는 UDP-glucose 산화 반응 또는 L-Ara4N 전이 반응의 *in vitro* 활성을 가짐을 측정하였다. pmrE 와 pmrF 유전자의 발현시킨 뒤 바나데이트가 들어있는 조건 하에서 폴리마이신에 대한 최소억제농도의 변화를 측정하였고 최소억제농도가 크게 상승하여 새로운 유전자들이 폴리마이신 내성에 기여함을 확인하였다.